

Higgs $\rightarrow \mu\tau$ as an indication for S_4 flavor symmetry

Miguel D. Campos,¹ A. E. Cárcamo Hernández,² H. Päs,³ and E. Schumacher³

¹*Max-Planck-Institut für Kernphysik, Saupfercheckweg 1, 69117 Heidelberg, Germany*

²*Universidad Técnica Federico Santa María and Centro Científico-Tecnológico de Valparaíso
Casilla 110-V, Valparaíso, Chile*

³*Fakultät für Physik, Technische Universität Dortmund, 44221 Dortmund, Germany*

Lepton flavor violating Higgs decays can arise in flavor symmetry models where the Higgs sector is responsible for both the electroweak and the flavor symmetry breaking. Here we advocate an S_4 three-Higgs-doublet model where tightly constrained flavor changing neutral currents are suppressed by a remnant Z_3 symmetry. A small breaking of this Z_3 symmetry can explain the 2.4σ excess of Higgs decay final states with a $\mu\tau$ topology reported recently by CMS if the new neutral scalars are light. The model also predicts sizable rates for lepton flavor violating Higgs decays in the $e\tau$ and $e\mu$ channels because of the unifying S_4 flavor symmetry.

PACS numbers: 11.30.Hv, 14.60.-z, 14.80.Ec

I. INTRODUCTION

Lepton flavor violating (LFV) Higgs decays have been advocated as a harbinger of flavor symmetries explaining the large amount of lepton flavor mixing [1–4]. Indeed, substantial LFV Higgs couplings can arise quite naturally in such models as a consequence of the maximal atmospheric $\mu - \tau$ mixing in the Pontecorvo-Maki-Nakagawa-Sakata (PMNS) matrix. To manifest itself in the physical mass basis, a misalignment of the Higgs doublets, typically utilized to yield a realistic symmetry breaking pattern, is necessary. While the scalar sector in [1–4] decomposes into a Standard Model (SM)-like Higgs doublet and new exotic scalars experiencing LFV decays, in the following we present an S_4 flavor model where these states mix, resulting in sizable LFV decays of the SM-like Higgs boson. This is particularly interesting after the recent report by the CMS Collaboration of a 2.4σ anomaly in the $h \rightarrow \mu\tau$ channel with a best fit of $\text{Br}(h \rightarrow \mu\tau) \approx 0.84\%$ [5], which as a possible hint of new physics beyond the SM, has drawn some attention [6–12]. Notably, the discrete group S_4 has been shown to be the most natural flavor symmetry of the tribimaximal (TBM) mixing scheme in the leptonic sector, with purely group theoretical arguments [13–15], as well as in explicit flavor models [16–18]. Furthermore, together with the groups A_4 and $\Delta(27)$, the S_4 group is the smallest group containing an irreducible triplet representation that can accommodate the three fermion families of the SM. Nonsupersymmetric S_4 models based on TBM mixing but accommodating a large θ_{13} have been discussed e.g. in [19–21]. To evade bounds from the tightly constrained radiative decays $l_\alpha \rightarrow l_\beta \gamma$, we consider the special case in which S_4 is broken down to a residual Z_3 subgroup (see [2] in the context of the symmetry groups A_4 , T_7 , and $\Delta(27)$, referred to as lepton flavor triality or LFT for short). This discrete Z_3 symmetry is obtained when scalar doublets in the irreducible triplet representation $\mathbf{3}'$ of S_4 assume the specific vacuum alignment $(1, 1, 1)$ [16]. If only the charged lepton sector is considered, the distinct Z_3 quantum numbers prevent any mixing of the physical scalars in this model. The Z_3 symmetry is, however, broken to some degree by perturbations arising from other scalar S_4 triplets required to extend the model to quarks and neutrinos. These perturbations enable mixing between the scalars and consequently lead to LFV Higgs decays.

The measurement of $h \rightarrow \mu\tau$ can be translated into a bound on the combination of Yukawa couplings $|y_{\mu\tau}|^2 + |y_{\tau\mu}|^2$ [11]. These couplings directly affect predictions for constrained LFV processes such as $\tau \rightarrow \mu\gamma$ or $\tau \rightarrow 3\mu$ which can be used to set bounds on the scalar masses in our 3HDM.

The paper is structured as follows. In Sec. II we develop a model with LFT that leads to realistic fermion masses and mixings. In Sec. III we analyze the breaking of the Z_3 group associated with LFT and its consequences for Higgs decays. In particular we focus on the $h \rightarrow \mu\tau$ channel explaining the recent 2.4σ anomaly and summarize predictions of our model for other rare LFV processes. The $h \rightarrow \gamma\gamma$ rate is considered in Sec. IV and a summary is given in Sec. V.

II. THE MODEL

A. Charged leptons

In the following we use the charged lepton sector as a starting point to introduce the relevant scalar content. Some of the additional scalars needed to accommodate quarks and neutrinos have an effect on the lepton phenomenology,

which we can exploit to explain the excess in $h \rightarrow \mu\tau$ reported by CMS, as will be discussed in Sec. III. The particle assignments relevant for the charged lepton sector in the notation $(S_4, SU(2), Z_{12})$ are

$$\begin{aligned} L = (L_e, L_\mu, L_\tau) : (3', 2, 1), \quad \tau_R : (1, 1, -i), \quad (e_R, \mu_R) : (2, 1, e^{\frac{7i\pi}{6}}), \\ \phi = (\phi_1, \phi_2, \phi_3) : (3', 2, 1), \quad \eta_1 : (1, 1, e^{\frac{i\pi}{6}}), \quad \eta_2 : (1', 1, e^{\frac{i\pi}{6}}). \end{aligned} \quad (1)$$

The scalar fields ϕ_j ($j = 1, 2, 3$) and the left-handed fermion $SU(2)$ doublets are both assigned to an S_4 triplet representation $\mathbf{3}'$. The former break the electroweak (EW) symmetry of the SM by spontaneously acquiring VEVs at the EW scale. Such models are usually referred to as three-Higgs-doublet models (3HDMs) and have been extensively analyzed in the past, e.g., in [22, 23].

To describe the hierarchy among the charged fermion masses, we introduce two EW scalar singlets, η_1 and η_2 . For the VEVs of $\eta_{1,2}$ we assume $v_{\eta_{1,2}} = \lambda\Lambda$ with $\lambda \approx 0.22$, where Λ is a high scale defining the breakdown of our effective theory. By choosing suitable Z_{12} charges we ensure that the tau and muon mass arise from seven and nine dimensional Yukawa terms, respectively. The smallness of the electron mass on the other hand is explained by the destructive interference between the contributions coming from the nine dimensional Yukawa operators and by a small breaking of the universality of the corresponding Yukawa couplings. The Z_{12} , therefore, functions as a Froggatt–Nielsen-like symmetry by creating mass hierarchies in the lepton and quark sector with $\mathcal{O}(1)$ Yukawa couplings [24].

As a consequence of the particle assignments given in Eq. (1) the scalar potential $V(\phi)$ involving only the ϕ field is the general S_4 -invariant scalar potential of a 3HDM [23]. Since the singlet scalars are assumed to be very heavy, the mixing between ϕ_i and $\eta_{1,2}$ is suppressed. For simplicity we also assume a CP-conserving scalar potential with only real couplings as done in, e.g., [25]. The renormalizable low-energy scalar potential is

$$V(\phi) = -\mu_1^2 \sum_{i=1}^3 \phi_i^\dagger \phi_i + \alpha \left(\sum_{i=1}^3 \phi_i^\dagger \phi_i \right)^2 + \sum_{i,j=1, i \neq j}^3 (\beta(\phi_i^\dagger \phi_i)(\phi_j^\dagger \phi_j) + \gamma |\phi_i^\dagger \phi_j|^2 + \delta(\phi_i^\dagger \phi_j)^2) \quad (2)$$

with the low-energy scalar content given by

$$\phi_j = \left[\phi_j^+, \quad \frac{1}{\sqrt{2}} \left(\frac{v}{\sqrt{3}} + \phi_{jR}^0 + i\phi_{jI}^0 \right) \right]. \quad (3)$$

It includes three CP-even neutral scalars ϕ_{jR}^0 ($j = 1, 2, 3$), and three CP-odd neutral scalars ϕ_{jI}^0 , as well as three complex charged scalars (ϕ_j^\pm) , of which three degrees of freedom are absorbed by the W^\pm and Z gauge boson masses. The corresponding physical mass spectrum reads

$$\begin{aligned} m_{\phi_{(a,b)R}^0}^2 &= -\frac{v^2}{3}\kappa, & m_{\phi_{eR}^0}^2 &= \frac{v^2}{3}(3\alpha + 2\kappa), & m_{\phi_{(a,b)I}^0}^2 &= -v^2\delta, \\ m_{\phi_{a,b}^\pm}^2 &= -v^2(\kappa - \beta), & m_{\phi_{eI}^0}^2 &= 0, & m_{\phi_c^\pm}^2 &= 0, \end{aligned} \quad (4)$$

with $\kappa := \beta + \gamma + \delta$.

The mass eigenstates $\phi_{a,b,c}$ are given by the following linear combinations of the S_4 basis scalars $\phi_{1,2,3}$:

$$\phi_a = \frac{1}{\sqrt{2}}(\phi_3 - \phi_2), \quad \phi_b = \frac{1}{\sqrt{6}}(2\phi_1 - \phi_2 - \phi_3), \quad \phi_c = \frac{1}{\sqrt{3}}(\phi_1 + \phi_2 + \phi_3). \quad (5)$$

These equations hold for the charged, CP-even and CP-odd components of ϕ , and they imply that

$$\langle \phi_a \rangle = \langle \phi_b \rangle = 0 \quad \text{and} \quad \langle \phi_c \rangle = v. \quad (6)$$

The fact that ϕ_c is the only mass eigenstate from the S_4 triplet acquiring a VEV proves essential for LFT. Along with the degeneracy of the scalars $\phi_{(a,b)R}^0$ (cf. Eq. (4)), it suggests that ϕ_{eR}^0 can be identified as the SM Higgs particle found at the LHC with a mass of approximately 125 GeV.

Using Eq. (5) we obtain the three- and four-point vertices of the physical scalars and the gauge bosons W^\pm, Z^0 and A from the kinetic terms of the Lagrangian. In the case of the three-point interactions, the only induced decay channels are $\phi_{eR}^0 \rightarrow W^+W^-$ and $\phi_{eR}^0 \rightarrow (Z^0)^2$. Hence, the SM-like Higgs ϕ_{eR}^0 is the only physical scalar giving masses to the SM gauge bosons with SM couplings. As a consequence, the masses of the neutral scalars $\phi_{(a,b)R}^0$ are not constrained by the usual Higgs searches performed in the LEP and LHC experiments [26, 27].

The relevant $S_4 \otimes Z_{12}$ -invariant Yukawa terms for the charged leptons

$$\mathcal{L} \supset y_1 [L\phi]_1 \tau_R \frac{\eta_1^3 + \varepsilon_0 \eta_1 \eta_2^2}{\Lambda^3} + y_2 [L\phi]_2 \left(\frac{e_R}{\mu_R} \right) \frac{\eta_1^5 + \varepsilon_1 \eta_1^3 \eta_2^2 + \varepsilon_2 \eta_1 \eta_2^4}{\Lambda^5} + y_3 [L\phi]_2 \left(\frac{e_R}{\mu_R} \right) \frac{\eta_2^5 + \varepsilon_3 \eta_2^3 \eta_1^2 + \varepsilon_4 \eta_2 \eta_1^4}{\Lambda^5} \quad (7)$$

lead to the following mass matrix for charged leptons:

$$M_l = \frac{1}{\sqrt{2}} \begin{pmatrix} v_1 (\tilde{y}_2 - \tilde{y}_3) \lambda^5 & v_1 (\tilde{y}_2 + \tilde{y}_3) \lambda^5 & v_1 \tilde{y}_1 \lambda^3 \\ v_2 \omega^2 (\tilde{y}_2 - \tilde{y}_3) \lambda^5 & v_2 \omega (\tilde{y}_2 + \tilde{y}_3) \lambda^5 & v_2 \tilde{y}_1 \lambda^3 \\ v_3 \omega (\tilde{y}_2 - \tilde{y}_3) \lambda^5 & v_3 \omega^2 (\tilde{y}_2 + \tilde{y}_3) \lambda^5 & v_3 \tilde{y}_1 \lambda^3 \end{pmatrix} \quad (8)$$

$$= v \frac{1}{\sqrt{6}} \begin{pmatrix} 1 & 1 & 1 \\ \omega^2 & \omega & 1 \\ \omega & \omega^2 & 1 \end{pmatrix} \text{diag}((\tilde{y}_2 - \tilde{y}_3) \lambda^5, (\tilde{y}_2 + \tilde{y}_3) \lambda^5, \tilde{y}_1 \lambda^3) \quad (9)$$

with $v_1 = v_2 = v_3 = \frac{v}{\sqrt{3}}$, $\omega = e^{2i\pi/3}$ and $\tilde{y}_1, \tilde{y}_2, \tilde{y}_3$ given by

$$\tilde{y}_1 = (1 + \varepsilon_0) y_1, \quad \tilde{y}_2 = (1 + \varepsilon_1 + \varepsilon_2) y_2, \quad \tilde{y}_3 = (1 + \varepsilon_3 + \varepsilon_4) y_3, \quad (10)$$

where the dimensionless couplings $y_1, y_2, y_3, \varepsilon_0, \varepsilon_1, \varepsilon_2, \varepsilon_3$ and ε_4 are $\mathcal{O}(1)$ parameters. Consequently the charged lepton masses are

$$m_e = (\tilde{y}_2 - \tilde{y}_3) \lambda^5 \frac{v}{\sqrt{2}}, \quad m_\mu = (\tilde{y}_2 + \tilde{y}_3) \lambda^5 \frac{v}{\sqrt{2}}, \quad m_\tau = \tilde{y}_1 \lambda^3 \frac{v}{\sqrt{2}}. \quad (11)$$

The mass hierarchy $m_e, m_\mu \ll m_\tau$, therefore, is a natural consequence of our model.

Equation (8) shows a characteristic feature of LFT that the mass basis of the charged leptons coincides with the Z_3 basis; i.e., the charged lepton fields can be identified as Z_3 eigenstates $e \sim 1, \mu \sim \omega^2, \tau \sim \omega$.

The structures for the couplings of the charged leptons to the physical scalars ϕ_{aR}^0, ϕ_{bR}^0 and ϕ_{cR}^0 are given by

$$Y_{(a)b} = (i) \frac{1}{v\sqrt{2}} \begin{pmatrix} 0 & m_\mu \omega^2 & (-)m_\tau \omega \\ (-)m_e \omega & 0 & m_\tau \omega^2 \\ m_e \omega^2 & (-)m_\mu \omega & 0 \end{pmatrix}, \quad Y_c = \frac{1}{v} \begin{pmatrix} m_e & 0 & 0 \\ 0 & m_\mu & 0 \\ 0 & 0 & m_\tau \end{pmatrix}, \quad (12)$$

where the factors in parentheses apply only to the structure of Y_a . As can be seen from Eq. (12), ϕ_c only couples diagonally to the charged leptons and, hence, should be uncharged under Z_3 . This can be understood by expressing the fields $\phi_{a,b,c}$ in terms of the Z_3 eigenstates

$$\begin{pmatrix} \phi_x \\ \phi_y \\ \phi_z \end{pmatrix} = \frac{1}{\sqrt{3}} \begin{pmatrix} 1 & 1 & 1 \\ 1 & \omega^2 & \omega \\ 1 & \omega & \omega^2 \end{pmatrix} \begin{pmatrix} \phi_1 \\ \phi_2 \\ \phi_3 \end{pmatrix} \quad \text{with } \phi_{x,y,z} \sim 1, \omega, \omega^2 \quad (13)$$

and consequently realizing that

$$\phi_c \equiv \phi_x, \quad \phi_b \equiv \frac{1}{\sqrt{2}}(\phi_y + \phi_z), \quad \phi_a \equiv \frac{1}{\sqrt{2}}(\phi_y - \phi_z). \quad (14)$$

Considering that ϕ_c is the only mass eigenstate from the ϕ S_4 triplet that acquires a VEV (cf. Eq. (6)), Z_3 remains unbroken at this point.

B. Neutrino sector

To generate the neutrino masses via a type I seesaw mechanism, we extend the SM particle content by two heavy Majorana neutrinos N_{1R} and N_{2R} as well as four S_4 triplets scalar fields χ, ξ, σ and ζ , which are singlets under $SU(2)$. Additionally we employ two Z_2 symmetries to enforce a specific mass pattern and decouple the scalars from interactions with the other fermion sectors. The corresponding $S_4 \otimes Z_2 \otimes Z'_2 \otimes Z_{12}$ assignments are

$$\begin{aligned} N_{1R} &: (1, -1, 1, 1), & N_{2R} &: (1, -1, -1, 1), \\ \chi &: (3', -1, 1, 1), & \xi &: (3, -1, 1, 1), & \sigma &: (3', -1, -1, 1), & \zeta &: (3, -1, -1, 1). \end{aligned} \quad (15)$$

Therefore the relevant $S_4 \otimes Z_2 \otimes Z'_2 \otimes Z_{12}$ -invariant neutrino Yukawa terms read

$$\begin{aligned} \mathcal{L} \supset & y_1^{(\nu)} [L\phi]_{3'} N_{1R} \frac{\chi}{\Lambda} + y_2^{(\nu)} [L\phi]_3 N_{1R} \frac{\xi}{\Lambda} + y_3^{(\nu)} [L\phi]_{3'} N_{2R} \frac{\sigma}{\Lambda} + y_4^{(\nu)} [L\phi]_3 N_{2R} \frac{\zeta}{\Lambda} + \frac{y_5^{(\nu)}}{\Lambda} L [\phi\chi]_{3'} N_{1R} \\ & + \frac{y_6^{(\nu)}}{\Lambda} L [\phi\xi]_{3'} N_{1R} + \frac{y_7^{(\nu)}}{\Lambda} L [\phi\sigma]_{3'} N_{2R} + \frac{y_8^{(\nu)}}{\Lambda} L [\phi\zeta]_{3'} N_{2R} + M_1 \bar{N}_{1R} N_{1R}^c + M_2 \bar{N}_{2R} N_{2R}^c. \end{aligned} \quad (16)$$

With the VEV patterns of the scalar fields χ , ξ , σ and ζ

$$\langle \chi \rangle = v_\chi (1, 0, 0), \quad \langle \xi \rangle = v_\xi (1, 0, 0), \quad \langle \sigma \rangle = v_\sigma (0, i, 0), \quad \langle \zeta \rangle = v_\zeta (0, 1, 0) \quad (17)$$

and the simplification

$$y_1^{(\nu)} = y_2^{(\nu)} = y_5^{(\nu)} = y_6^{(\nu)} = y^{(\nu)}, \quad (18)$$

it follows that the full 5×5 neutrino mass matrix is

$$M_L^{(\nu)} = \begin{pmatrix} 0_{3 \times 3} & M_\nu^D \\ (M_\nu^D)^T & M_R \end{pmatrix}, \quad (19)$$

where

$$M_\nu^D = \begin{pmatrix} 0 & \lambda \left[(y_4^{(\nu)} + y_6^{(\nu)}) - i (y_3^{(\nu)} + y_7^{(\nu)}) \right] \\ 4\lambda y^{(\nu)} & 0 \\ 0 & \lambda \left[(y_4^{(\nu)} + y_6^{(\nu)}) + i (y_3^{(\nu)} + y_7^{(\nu)}) \right] \end{pmatrix} \frac{v}{\sqrt{3}} = \begin{pmatrix} 0 & ae^{i\tau} \\ b & 0 \\ 0 & ae^{-i\tau} \end{pmatrix} \frac{v}{\sqrt{3}}, \quad M_R = \begin{pmatrix} M_1 & 0 \\ 0 & M_2 \end{pmatrix},$$

$$a = \lambda \sqrt{(y_4^{(\nu)} + y_6^{(\nu)})^2 + (y_3^{(\nu)} + y_7^{(\nu)})^2}, \quad b = 4\lambda y^{(\nu)}, \quad \tan \tau = -\frac{y_3^{(\nu)} + y_7^{(\nu)}}{y_4^{(\nu)} + y_6^{(\nu)}}. \quad (20)$$

Since $(M_R)_{ii} \gg v$, the light neutrino mass matrix arises from a type I seesaw mechanism and is given by:

$$M_L^{(\nu)} = M_\nu^D M_R^{-1} (M_\nu^D)^T = \begin{pmatrix} a^2 e^{2i\tau} & 0 & a^2 \\ 0 & b^2 \frac{M_2}{M_1} & 0 \\ a^2 & 0 & a^2 e^{-2i\tau} \end{pmatrix} \frac{v^2}{3M_2} = \begin{pmatrix} Ae^{2i\tau} & 0 & A \\ 0 & B & 0 \\ A & 0 & Ae^{-2i\tau} \end{pmatrix} \quad (21)$$

with

$$A = a^2 \frac{v^2}{3M_2}, \quad B = b^2 \frac{v^2}{3M_1}. \quad (22)$$

It is worth mentioning that the neutrino mass matrix depends only on three effective parameters, A , B and τ , of which A and B are inverse proportional to M_2 and M_1 , respectively. Furthermore, the smallness of the active neutrino masses arises from their inverse scaling with the large Majorana neutrino masses as well as from the quadratic dependence of the neutrino Yukawa couplings, which is a characteristic feature of the type I seesaw mechanism. The right handed Majorana neutrinos obtain large masses due to their Yukawa interactions with EW scalar singlets, which acquire VEVs much larger than the electroweak scale.

The squared mass matrix $M_L^{(\nu)} (M_L^{(\nu)})^\dagger$ is diagonalized by a unitary rotation matrix V_ν as follows [28–31]:

$$V_\nu^\dagger M_\nu^{(1)} (M_\nu^{(1)})^\dagger V_\nu = \begin{pmatrix} m_1^2 & 0 & 0 \\ 0 & m_2^2 & 0 \\ 0 & 0 & m_3^2 \end{pmatrix}, \quad \text{with} \quad V_\nu = \begin{pmatrix} \cos \psi & 0 & \sin \psi e^{-i\phi} \\ 0 & 1 & 0 \\ -\sin \psi e^{i\phi} & 0 & \cos \psi \end{pmatrix}, \quad \psi = \pm \frac{\pi}{4}, \quad \phi = -2\tau, \quad (23)$$

where $\psi = +\pi/4$ and $\psi = -\pi/4$ correspond to the normal (NH) and inverted (IH) mass hierarchies, respectively. The light active neutrino masses for NH and IH are:

$$\text{NH} : \psi = +\frac{\pi}{4} : \quad m_{\nu_1} = 0, \quad m_{\nu_2} = B, \quad m_{\nu_3} = 2|A|, \quad (24)$$

$$\text{IH} : \psi = -\frac{\pi}{4} : \quad m_{\nu_1} = 2|A|, \quad m_{\nu_2} = B, \quad m_{\nu_3} = 0. \quad (25)$$

By combining Eqs. (8) and (23) we obtain the PMNS leptonic mixing matrix

$$U = V_{lL}^\dagger V_\nu = \begin{pmatrix} \frac{\cos \psi}{\sqrt{3}} - \frac{e^{i\phi - \frac{2i\pi}{3}} \sin \psi}{\sqrt{3}} & \frac{e^{\frac{2i\pi}{3}}}{\sqrt{3}} & \frac{e^{-\frac{2i\pi}{3}} \cos \psi}{\sqrt{3}} + \frac{e^{-i\phi} \sin \psi}{\sqrt{3}} \\ \frac{\cos \psi}{\sqrt{3}} - \frac{e^{i\phi + \frac{2i\pi}{3}} \sin \psi}{\sqrt{3}} & \frac{e^{-\frac{2i\pi}{3}}}{\sqrt{3}} & \frac{e^{\frac{2i\pi}{3}} \cos \psi}{\sqrt{3}} + \frac{e^{-i\phi} \sin \psi}{\sqrt{3}} \\ \frac{\cos \psi}{\sqrt{3}} - \frac{e^{i\phi} \sin \psi}{\sqrt{3}} & \frac{1}{\sqrt{3}} & \frac{\cos \psi}{\sqrt{3}} + \frac{e^{-i\phi} \sin \psi}{\sqrt{3}} \end{pmatrix}, \quad (26)$$

which only depends on a single parameter ϕ , whereas the neutrino mass squared splittings are determined by the parameters A and B .

Furthermore, we find that the lepton mixing angles are given by:

$$\sin^2 \theta_{12} = \frac{|U_{e2}|^2}{1 - |U_{e3}|^2} = \frac{2}{4 \pm (\cos \phi - \sqrt{3} \sin \phi)}, \quad (27)$$

$$\sin^2 \theta_{13} = |U_{e3}|^2 = \frac{1}{6} \left[2 \mp (\cos \phi - \sqrt{3} \sin \phi) \right], \quad (28)$$

$$\sin^2 \theta_{23} = \frac{|U_{\mu 3}|^2}{1 - |U_{e3}|^2} = \frac{2 \mp (\cos \phi + \sqrt{3} \sin \phi)}{4 \pm (\cos \phi - \sqrt{3} \sin \phi)}. \quad (29)$$

The Jarlskog invariant and the CP-violating phase are given by [32]

$$J = \text{Im} (U_{e1} U_{\mu 2} U_{e2}^* U_{\mu 1}^*) = \frac{1}{6\sqrt{3}} \cos 2\psi, \quad \sin \delta = \frac{8J}{\cos \theta_{13} \sin 2\theta_{12} \sin 2\theta_{23} \sin 2\theta_{13}}. \quad (30)$$

Since $\psi = \pm \frac{\pi}{4}$, we predict $J = 0$ and $\delta = 0$, which corresponds to CP conservation in neutrino oscillations.

In what follows we adjust the three free effective parameters ϕ , A and B of the light neutrino sector to accommodate the experimental values of three leptonic mixing parameters and two neutrino mass squared splittings, reported in Tables I and II for NH and IH, respectively. We fit the ϕ parameter to adjust the values of the leptonic mixing parameters $\sin^2 \theta_{ij}$, whereas A and B are given by

$$\text{NH} : m_{\nu_1} = 0, \quad m_{\nu_2} = B = \sqrt{\Delta m_{21}^2} \approx 9 \text{ meV}, \quad m_{\nu_3} = 2|A| = \sqrt{\Delta m_{31}^2} \approx 50 \text{ meV}; \quad (31)$$

$$\text{IH} : m_{\nu_2} = B = \sqrt{\Delta m_{21}^2 + \Delta m_{13}^2} \approx 50 \text{ meV}, \quad m_{\nu_1} = 2|A| = \sqrt{\Delta m_{13}^2} \approx 49 \text{ meV}, \quad m_{\nu_3} = 0, \quad (32)$$

resulting from Eqs. (24) and (25), the definition $\Delta m_{ij}^2 = m_i^2 - m_j^2$, and the best-fit values of Δm_{ij}^2 from Tables I and II for NH and IH, respectively.

By varying ϕ we obtain the following best-fit result:

$$\text{NH} : \phi = -0.453\pi, \quad \sin^2 \theta_{12} \approx 0.34, \quad \sin^2 \theta_{23} \approx 0.61, \quad \sin^2 \theta_{13} \approx 0.0232; \quad (33)$$

$$\text{IH} : \phi = 0.546\pi, \quad \sin^2 \theta_{12} \approx 0.34, \quad \sin^2 \theta_{23} \approx 0.61, \quad \sin^2 \theta_{13} \approx 0.024. \quad (34)$$

Comparing Eqs. (33) and (34) with Tables I and II, we obtain $\sin^2 \theta_{13}$ and $\sin^2 \theta_{23}$ in excellent agreement with the experimental data, for both mass hierarchies, whereas $\sin^2 \theta_{12}$ deviates 2σ away from its best-fit values. Consequently, our predictions for the neutrino mass squared splittings and leptonic mixing parameters are in very good agreement with the experimental data on neutrino oscillations. Furthermore, our model predicts the absence of CP violation in neutrino oscillations.

Parameter	$\Delta m_{21}^2 (10^{-5} \text{ eV}^2)$	$\Delta m_{31}^2 (10^{-3} \text{ eV}^2)$	$(\sin^2 \theta_{12})_{\text{exp}}$	$(\sin^2 \theta_{23})_{\text{exp}}$	$(\sin^2 \theta_{13})_{\text{exp}}$
Best fit	7.60	2.48	0.323	0.567	0.0234
1 σ range	7.42 – 7.79	2.41 – 2.53	0.307 – 0.339	0.439 – 0.599	0.0214 – 0.0254
2 σ range	7.26 – 7.99	2.35 – 2.59	0.292 – 0.357	0.413 – 0.623	0.0195 – 0.0274
3 σ range	7.11 – 8.11	2.30 – 2.65	0.278 – 0.375	0.392 – 0.643	0.0183 – 0.0297

Table I: Range for experimental values of neutrino mass squared splittings and leptonic mixing parameters, taken from Ref. [33], for the case of normal hierarchy.

C. Quark sector

To obtain realistic quark masses and mixings we add SM scalar singlets, i.e., two S_4 triplets, ρ and φ , and three S_4 singlets Ω_1 , Ω_2 and Ω_3 . Again we use a Z_2'' symmetry to decouple these scalars from the other fermion sectors,

Parameter	$\Delta m_{21}^2 (10^{-5} \text{eV}^2)$	$\Delta m_{13}^2 (10^{-3} \text{eV}^2)$	$(\sin^2 \theta_{12})_{\text{exp}}$	$(\sin^2 \theta_{23})_{\text{exp}}$	$(\sin^2 \theta_{13})_{\text{exp}}$
Best fit	7.60	2.38	0.323	0.573	0.0240
1σ range	7.42 – 7.79	2.32 – 2.43	0.307 – 0.339	0.530 – 0.598	0.0221 – 0.0259
2σ range	7.26 – 7.99	2.26 – 2.48	0.292 – 0.357	0.432 – 0.621	0.0202 – 0.0278
3σ range	7.11 – 8.11	2.20 – 2.54	0.278 – 0.375	0.403 – 0.640	0.0183 – 0.0297

Table II: Range for experimental values of neutrino mass squared splittings and leptonic mixing parameters, taken from Ref. [33], for the case of inverted hierarchy.

whereas a Z_6 symmetry accounts for the top and bottom mass hierarchy. The $S_4 \otimes Z_2'' \otimes Z_6 \otimes Z_{12}$ assignments are:

$$\begin{aligned} t_R : (1, 1, 1, 1), \quad c_R : (1, 1, 1, 1), \quad u_R : (1, 1, 1, -1), \quad b_R : (1, 1, -1, 1), \quad s_R : (1, 1, -1, 1), \quad d_R : (1, 1, -1, -1), \\ Q : (3', -1, 1, 1), \quad \rho : (3', -1, 1, 1), \quad \varphi : (3, -1, 1, 1), \quad \Omega_1 : (1, 1, 1, i), \quad \Omega_2 : (1, -1, 1, \omega^{\frac{1}{2}}), \quad \Omega_3 : (1, 1, \omega^{\frac{1}{2}}, 1) \end{aligned} \quad (35)$$

with the VEV patterns of the scalar fields ρ , φ , Ω_1 , Ω_2 and Ω_3

$$\langle \rho \rangle = v_\rho (i, 0, 0), \quad \langle \varphi \rangle = v_\varphi (1, 0, 0), \quad \langle \Omega_1 \rangle = v_{\Omega_1}, \quad \langle \Omega_2 \rangle = v_{\Omega_2} e^{i\theta_{\Omega_2}}, \quad \langle \Omega_3 \rangle = v_{\Omega_3}. \quad (36)$$

The Z_{12} symmetry creates a hierarchy among the columns of the quark mass matrices which leads to the quark mass hierarchies observed in experiments without additional fine-tuning. The relevant $S_4 \otimes Z_2'' \otimes Z_6 \otimes Z_{12}$ -invariant Yukawa terms for the up- and down-type quarks are given in Appendix C. Using the S_4 multiplication rules listed in Appendix A, it follows that the quark mass matrices are given by

$$M_q = \begin{pmatrix} C_q e^{i\theta_{1q}} & 0 & 0 \\ D_q e^{-i\theta_{2q}} & E_q e^{-i\theta_{3q}} & F_q e^{-i\theta_{4q}} \\ D_q e^{i\theta_{2q}} & E_q e^{i\theta_{3q}} & F_q e^{i\theta_{4q}} \end{pmatrix}, \quad q = U, D. \quad (37)$$

Then the quark mass matrices satisfy the following relation:

$$M_q M_q^\dagger = \begin{pmatrix} C_q e^{i\theta_{1q}} & 0 & 0 \\ D_q e^{-i\theta_{2q}} & E_q e^{-i\theta_{3q}} & F_q e^{-i\theta_{4q}} \\ D_q e^{i\theta_{2q}} & E_q e^{i\theta_{3q}} & F_q e^{i\theta_{4q}} \end{pmatrix} \begin{pmatrix} C_q e^{-i\theta_{1q}} & D_q e^{i\theta_{2q}} & D_q e^{-i\theta_{2q}} \\ 0 & E_q e^{i\theta_{3q}} & E_q e^{-i\theta_{3q}} \\ 0 & F_q e^{i\theta_{4q}} & F_q e^{-i\theta_{4q}} \end{pmatrix} \quad (38)$$

$$= \begin{pmatrix} C_q^2 & C_q D_q e^{i(\theta_{1q} + \theta_{2q})} & C_q D_q e^{i(\theta_{1q} - \theta_{2q})} \\ C_q D_q e^{-i(\theta_{1q} + \theta_{2q})} & D_q^2 + E_q^2 + F_q^2 & D_q^2 e^{-2i\theta_{2q}} + E_q^2 e^{-2i\theta_{3q}} + F_q^2 e^{-2i\theta_{4q}} \\ C_q D_q e^{i(\theta_{1q} - \theta_{2q})} & D_q^2 e^{2i\theta_{2q}} + E_q^2 e^{2i\theta_{3q}} + F_q^2 e^{2i\theta_{4q}} & D_q^2 + E_q^2 + F_q^2 \end{pmatrix} \quad (39)$$

$$= \begin{pmatrix} X_q & Y_q e^{i\theta_{aq}} & Y_q e^{i\theta_{bq}} \\ Y_q e^{-i\theta_{aq}} & U_q & V_q e^{i\theta_{cq}} \\ Y_q e^{-i\theta_{bq}} & V_q e^{-i\theta_{cq}} & U_q \end{pmatrix} \quad (40)$$

where X_q , Y_q , V_q and U_q are real parameters. For the sake of simplicity we assume $\theta_{cq} = \theta_{bq} - \theta_{aq}$, so that the relevant physical part of the quark mass matrices can be rewritten as follows:

$$M_q M_q^\dagger = P_q J_q P_q^\dagger, \quad P_q = \begin{pmatrix} 1 & 0 & 0 \\ 0 & e^{-i\theta_{aq}} & 0 \\ 0 & 0 & e^{-i\theta_{cq}} \end{pmatrix}, \quad J_q = \begin{pmatrix} X_q & Y_q & Y_q \\ Y_q & U_q & V_q \\ Y_q & V_q & U_q \end{pmatrix}. \quad (41)$$

The matrix J_q corresponds to a modification of the Fukuyama-Nishiura texture proposed in [34] and is diagonalized by an orthogonal matrix R_q as follows:

$$R_q J_q R_q^T = \text{diag}(-m_{q1}^2, m_{q2}^2, m_{q3}^2), \quad R_q = \begin{pmatrix} c_q & s_q & 0 \\ -\frac{s_q}{\sqrt{2}} & \frac{c_q}{\sqrt{2}} & -\frac{1}{\sqrt{2}} \\ -\frac{s_q}{\sqrt{2}} & \frac{c_q}{\sqrt{2}} & \frac{1}{\sqrt{2}} \end{pmatrix}, \quad (42)$$

where:

$$c_q = \sqrt{\frac{m_{q_2}^2 - X_q}{m_{q_2}^2 + m_{q_1}^2}}, \quad s_q = \sqrt{\frac{m_{q_1}^2 + X_q}{m_{q_2}^2 + m_{q_1}^2}} \quad (43)$$

with the quark masses

$$-m_{q_1}^2 = \frac{1}{2} \left(U_q + V_q + X_q - \sqrt{(X_q - U_q - V_q)^2 + 8Y_q^2} \right), \quad (44)$$

$$m_{q_2}^2 = \frac{1}{2} \left(U_q + V_q + X_q + \sqrt{(X_q - U_q - V_q)^2 + 8Y_q^2} \right), \quad (45)$$

$$m_{q_3}^2 = U_q - V_q. \quad (46)$$

Furthermore, for the CKM quark mixing matrix we obtain

$$K = O_U^T P_{UD} O_D = \begin{pmatrix} c_U c_D + \frac{1}{2} s_U s_D (e^{i\vartheta} + e^{i\varrho}) & c_U s_D - \frac{1}{2} s_U c_D (e^{i\vartheta} + e^{i\varrho}) & \frac{1}{2} s_U (e^{i\vartheta} - e^{i\varrho}) \\ s_U c_D - \frac{1}{2} c_U s_D (e^{i\vartheta} + e^{i\varrho}) & s_U s_D + \frac{1}{2} c_U c_D (e^{i\vartheta} + e^{i\varrho}) & \frac{1}{2} c_U (e^{i\vartheta} - e^{i\varrho}) \\ \frac{1}{2} s_D (e^{i\vartheta} - e^{i\varrho}) & \frac{1}{2} c_D (e^{i\vartheta} - e^{i\varrho}) & \frac{1}{2} (e^{i\vartheta} + e^{i\varrho}) \end{pmatrix}, \quad (47)$$

where $P_{UD} = P_U^\dagger P_D = \text{diag}(1, e^{i\vartheta}, e^{i\varrho})$, with $\vartheta = \theta_{aU} - \theta_{aD}$ and $\varrho = \theta_{bU} - \theta_{bD}$.

Using the values of the quark masses at the M_Z scale shown in Table III and varying the parameters $X_{U,D}$, ϑ and ϱ we fit the magnitudes of the CKM matrix elements, the CP-violating phase and the Jarlskog invariant J to the experimental values shown in Table IV. The values of the quark masses at the M_Z scale have been taken from Ref. [35], whereas the experimental values of the CKM magnitudes and the Jarlskog invariant J are taken from Ref. [36].

Quark masses	Experimental Value
$m_d(\text{MeV})$	$2.9^{+0.5}_{-0.4}$
$m_s(\text{MeV})$	$57.7^{+16.8}_{-15.7}$
$m_b(\text{MeV})$	2820^{+90}_{-40}
$m_u(\text{MeV})$	$1.45^{+0.56}_{-0.45}$
$m_c(\text{MeV})$	635 ± 86
$m_t(\text{MeV})$	$172.1 \pm 0.6 \pm 0.9$

Table III: Experimental values of the quark masses at the M_Z scale. [35].

Observable	Fukuyama like texture	Experimental Value
$ V_{ud} $	0.974	0.97427 ± 0.00015
$ V_{us} $	0.225	0.22534 ± 0.00065
$ V_{ub} $	0.00351	$0.00351^{+0.00015}_{-0.00014}$
$ V_{cd} $	0.225	0.22520 ± 0.00065
$ V_{cs} $	0.973	0.97344 ± 0.00016
$ V_{cb} $	0.0412	$0.0412^{+0.0011}_{-0.0005}$
$ V_{td} $	0.00867	$0.00867^{+0.00029}_{-0.00031}$
$ V_{ts} $	0.0404	$0.0404^{+0.0011}_{-0.0005}$
$ V_{tb} $	0.999	$0.999146^{+0.000021}_{-0.000046}$
J	2.96×10^{-5}	$(2.96^{+0.20}_{-0.16}) \times 10^{-5}$
δ	69.2°	68°

Table IV: Experimental CKM magnitudes and Jarlskog invariant compared with results obtained from our fit.

Using the values

$$X_U = 2.90 \times 10^{-3} \text{ GeV}^2, \quad X_D = 1.38 \times 10^{-4} \text{ GeV}^2, \quad \vartheta = 87.9^\circ, \quad \varrho = 92.6^\circ, \quad (48)$$

the obtained magnitudes of the CKM matrix elements, the CP-violating phase and the Jarlskog invariant are in excellent agreement with the experimental data.

III. Z_3 BREAKING

A. Scalar sector

The S_4 symmetry of the model is broken down to a residual Z_3 symmetry once the S_4 triplet ϕ acquires VEVs in the direction $v(1, 1, 1)$. However, perturbations can arise from other scalars without a mechanism to protect the necessary VEV alignments, e.g., from a scalar triplet χ acquiring VEVs in the $v_\chi(1, 0, 0)$ direction to generate neutrino masses and mixings (cf. Eqs. (15–17)). These perturbations are caused by quartic interactions of the form $(\phi^\dagger \phi)(\chi^\dagger \chi)$ that appear in the scalar potential and cannot be forbidden by a flavor symmetry since the combinations $\phi^\dagger \phi$ and $\chi^\dagger \chi$ are always invariant.

In our model the scalar triplet responsible for the charged lepton masses is ϕ with $\langle \phi \rangle = v(1, 1, 1)$, assigned to $(3', 2)$ under $S_4 \otimes SU(2)$, whereas several scalars responsible for mixings in the quark and neutrino sector cause deviations from this alignment through quartic interactions with ϕ . If we assume a VEV hierarchy among those scalars to simplify the discussion, i.e., $v_\rho, v_\varphi \gg v_\chi, v_\xi, v_\sigma, v_\zeta$, the perturbations coming from scalars involved in neutrino interactions can be neglected. The remaining fields being

$$\rho : (3', 1), \quad \varphi : (3, 1) \quad \text{with} \quad \langle \rho \rangle = v_\rho(i, 0, 0), \quad \langle \varphi \rangle = v_\varphi(1, 0, 0).$$

Thus, the relevant cross couplings in the scalar potential are

$$V_{\text{int}} \supset \sum_{i=\mathbf{1}, \mathbf{2}, \mathbf{3}, \mathbf{3}'} (\phi^\dagger \phi)_i [\lambda_{\rho_i} (\rho^\dagger \rho)_i + \lambda_{\varphi_i} (\varphi^\dagger \varphi)_i], \quad (49)$$

where $i = \mathbf{1}, \mathbf{2}, \mathbf{3}, \mathbf{3}'$ denotes the corresponding S_4 contraction. Eventually only the $\mathbf{2}$ -contractions, e.g., $\sum_{j,k=1, j \neq k}^3 2|\phi_j|^2 |\rho_j|^2 - |\phi_j|^2 |\rho_k|^2$, result in perturbations of the Z_3 conserving VEV alignment $v(1, 1, 1)$ as the other contractions are invariant under the Z_3 conserving generator after the scalars ρ and φ acquire their VEVs. Therefore we only need to consider the following terms in the scalar potential to analyze the breaking of Z_3

$$V_{\text{int}} \supset (\phi^\dagger \phi)_{\mathbf{2}} [\lambda_\rho (\rho^\dagger \rho)_{\mathbf{2}} + \lambda_\varphi (\varphi^\dagger \varphi)_{\mathbf{2}}] \quad (50)$$

$$= \sum_{j,k=1, j \neq k}^3 |\phi_j|^2 [\lambda_\rho (2|\rho_j|^2 - |\rho_k|^2) + \lambda_\varphi (2|\varphi_j|^2 - |\varphi_k|^2)]. \quad (51)$$

Assuming for simplicity that the coupling constants are the same order of magnitude, i.e., $\lambda_\rho \approx \lambda_\varphi \approx \lambda_s/2$, the VEV alignment of the triplet ϕ is approximately shifted by a perturbation ϵ in the following way

$$\langle \phi \rangle = v(1 + 2\epsilon, 1 - \epsilon, 1 - \epsilon), \quad (52)$$

where the contributions from ρ and φ are summarized in the parameter ϵ . Doing so, we adopt a similar approach as in [10], who recently analyzed a triality model based on an A_4 flavor symmetry.

As a consequence, one of the physical Higgs doublets which was initially inert before the breaking of Z_3 , $\langle \phi_b \rangle = 0$, now acquires a small VEV depending on the size of the perturbation parameter ϵ

$$\begin{pmatrix} \langle \phi_a \rangle \\ \langle \phi_b \rangle \\ \langle \phi_c \rangle \end{pmatrix} = \begin{pmatrix} 0 & -\frac{1}{\sqrt{2}} & \frac{1}{\sqrt{2}} \\ \frac{\sqrt{2}}{\sqrt{3}} & -\frac{1}{\sqrt{6}} & -\frac{1}{\sqrt{6}} \\ \frac{1}{\sqrt{3}} & \frac{1}{\sqrt{3}} & \frac{1}{\sqrt{3}} \end{pmatrix} \begin{pmatrix} \frac{v}{\sqrt{3}}(1 + 2\epsilon) \\ \frac{v}{\sqrt{3}}(1 - \epsilon) \\ \frac{v}{\sqrt{3}}(1 - \epsilon) \end{pmatrix} = v \begin{pmatrix} 0 \\ \sqrt{2}\epsilon \\ 1 \end{pmatrix}. \quad (53)$$

Following [10] we use the parametrization

$$\langle (\phi_a, \phi_b, \phi_c)^T \rangle = v(0, \sin \theta, \cos \theta), \quad (54)$$

where θ is given by a combination of parameters from the scalar potential to account for the deviation from LFT. From now onwards we will use the abbreviations $\sin \theta := s_\theta$ and $\cos \theta := c_\theta$.

The breaking of Z_3 induces new mixing of the doublets ϕ_b and ϕ_c which were initially mass eigenstates. The CP-odd neutral scalars $\phi_{(b,c),I}^0$ and the charged scalars $\phi_{b,c}^\pm$ mix via

$$\begin{pmatrix} H^\pm \\ \pi^\pm \end{pmatrix} = \begin{pmatrix} c_\theta & s_\theta \\ -s_\theta & c_\theta \end{pmatrix} \begin{pmatrix} \phi_b^\pm \\ \phi_c^\pm \end{pmatrix} \quad \text{and} \quad \begin{pmatrix} \eta_I^0 \\ \pi_I^0 \end{pmatrix} = \begin{pmatrix} c_\theta & s_\theta \\ -s_\theta & c_\theta \end{pmatrix} \begin{pmatrix} \phi_{b,I}^0 \\ \phi_{c,I}^0 \end{pmatrix}, \quad (55)$$

where π^\pm and π_I^0 are massless goldstone bosons. In the case of the CP-even neutral scalars the situation is more complicated and the mixing results in a mass splitting of the scalars which were initially degenerate in mass. The complete mass spectrum reads

$$m_{\phi_{a,I}^0}^2 = m_{\pi_I^0}^2 = -v^2\delta, \quad m_{\pi_I^0}^2 = 0, \quad (56)$$

$$m_{\phi_a^\pm}^2 = m_{H^\pm}^2 = -v^2(\kappa - \beta), \quad m_{\pi^\pm}^2 = 0, \quad (57)$$

$$m_{\phi_{a,R}^0}^2 = \frac{1}{6}v^2(-2 + 2\sqrt{2}c_\theta s_\theta + s_\theta^2)\kappa, \quad (58)$$

$$m_h^2 = \frac{1}{2}(v^2\alpha - m_{\phi_{a,R}^0}^2) + \Delta, \quad m_H^2 = \frac{1}{2}(v^2\alpha - m_{\phi_{a,R}^0}^2) - \Delta \quad (59)$$

$$\text{with} \quad \Delta = \frac{1}{6}v^2\sqrt{9(\alpha + \kappa)^2 + 3\kappa s_\theta \left[2\sqrt{2}c_\theta(\alpha + \kappa) - 3s_\theta(5\alpha + 3\kappa) \right] + \mathcal{O}(s_\theta^3)}. \quad (60)$$

Note that only the masses of the CP-even scalars depend on the perturbation parameter θ . Hence Z_3 breaking in this direction does not affect the phenomenology of the CP-odd and charged scalars in our triality model. In the triality limit $\theta \rightarrow 0$ the mixing vanishes and the original mass spectrum is recovered with $m_h^2 \xrightarrow{\theta \rightarrow 0} m_{\phi_{c,R}^0}^2$ and $m_H^2 \xrightarrow{\theta \rightarrow 0} m_{\phi_{b,R}^0}^2 = m_{\phi_{a,R}^0}^2$. Therefore the scalar h should play the role of the SM-like Higgs with $m_h \approx 125$ GeV, whereas H will be a new heavy Higgs as in regular two-Higgs-doublet models (2HDM). The mixing angle ϑ between the CP even neutral scalars is defined by

$$\begin{pmatrix} H \\ h \end{pmatrix} = \begin{pmatrix} c_\vartheta & s_\vartheta \\ -s_\vartheta & c_\vartheta \end{pmatrix} \begin{pmatrix} \phi_{b,R}^0 \\ \phi_{c,R}^0 \end{pmatrix} \quad \text{and} \quad (61)$$

$$\tan 2\vartheta = -\frac{4s_\theta(\sqrt{2}\kappa s_\theta - 2c_\theta(3\alpha + \kappa))}{6(-1 + 2s_\theta^2)\alpha + (-6 - 2\sqrt{2}c_\theta s_\theta + 11s_\theta^2)\kappa} \quad (62)$$

with $\vartheta \rightarrow 0$ for $\theta \rightarrow 0$ in the unbroken triality limit. In terms of the scalar masses $m_h \approx 125$ GeV and $m_{\phi_{a,R}^0} := m_a$ this is

$$\tan 2\vartheta = \frac{A}{B} \quad \text{with} \quad (63)$$

$$\begin{aligned} A &= s_\theta(c_\theta(4m_a^2m_h^2s_\theta^2(2 - 7s_\theta^2) + 4m_h^4(4 + 4s_\theta^2 - 7s_\theta^4) - 8m_a^4(2 - 5s_\theta^2 + 3s_\theta^4)) \\ &\quad - 4\sqrt{2}s_\theta(4m_h^4(2 - 3s_\theta^2 + s_\theta^4) + m_a^2m_h^2(2 - 7s_\theta^2 + 4s_\theta^4) + m_a^4(6 - 19s_\theta^2 + 15s_\theta^4))), \\ B &= 2m_a^2m_h^2(4 - 16s_\theta^2 + 17s_\theta^4 + 4\sqrt{2}c_\theta s_\theta^5 - 7s_\theta^6) \\ &\quad + m_h^4(-1 + 2s_\theta^2)(4 + 4s_\theta^2 - 7s_\theta^4 + 4\sqrt{2}c_\theta s_\theta(-2 + s_\theta^2)) \\ &\quad + m_a^4(-4 + 12s_\theta^2 - 11s_\theta^4 + 5s_\theta^6 - 2\sqrt{2}c_\theta s_\theta(4 - 14s_\theta^2 + 13s_\theta^4)). \end{aligned}$$

Since the mass of the scalar h is fixed, the mixing angle ϑ depends only on two parameters. Here we chose the perturbation angle θ and the mass of the exotic Higgs $\phi_{a,R}^0$. Through the relation $m_a^2 = v^2\alpha - (m_h^2 + m_H^2)$ one can alternatively display the results in terms of m_H , which is the heavy Higgs in our pseudo 2HDM.

B. Consequences for lepton mixing

As a consequence of the perturbed alignment $v(0, s_\theta, c_\theta)$ the mass matrix of the charged leptons takes the form

$$M_l = \frac{v}{\sqrt{6}} \begin{pmatrix} (c_\theta + \sqrt{2}s_\theta)(\tilde{y}_2 - \tilde{y}_3)\lambda^5 & (c_\theta + \sqrt{2}s_\theta)(\tilde{y}_2 + \tilde{y}_3)\lambda^5 & (c_\theta + \sqrt{2}s_\theta)\tilde{y}_1\lambda^3 \\ \frac{1}{2}(2c_\theta - \sqrt{2}s_\theta)(\tilde{y}_2 - \tilde{y}_3)\lambda^5\omega^2 & \frac{1}{2}(2c_\theta - \sqrt{2}s_\theta)(\tilde{y}_2 + \tilde{y}_3)\lambda^5\omega & \frac{1}{2}(2c_\theta - \sqrt{2}s_\theta)\tilde{y}_1\lambda^3 \\ \frac{1}{2}(2c_\theta - \sqrt{2}s_\theta)(\tilde{y}_2 - \tilde{y}_3)\lambda^5\omega & \frac{1}{2}(2c_\theta - \sqrt{2}s_\theta)(\tilde{y}_2 + \tilde{y}_3)\lambda^5\omega^2 & \frac{1}{2}(2c_\theta - \sqrt{2}s_\theta)\tilde{y}_1\lambda^3 \end{pmatrix} \quad (64)$$

$$= \frac{v}{\sqrt{2}} \underbrace{\frac{1}{\sqrt{3}} \begin{pmatrix} 1 & 1 & 1 \\ \omega^2 & \omega & 1 \\ \omega & \omega^2 & 1 \end{pmatrix}}_{U_\omega} \begin{pmatrix} c_\theta(\tilde{y}_2 - \tilde{y}_3)\lambda^5 & \frac{s_\theta(\tilde{y}_2 + \tilde{y}_3)\lambda^5}{\sqrt{2}} & \frac{s_\theta\tilde{y}_1\lambda^3}{\sqrt{2}} \\ \frac{s_\theta(\tilde{y}_2 - \tilde{y}_3)\lambda^5}{\sqrt{2}} & c_\theta(\tilde{y}_2 + \tilde{y}_3)\lambda^5 & \frac{s_\theta\tilde{y}_1\lambda^3}{\sqrt{2}} \\ \frac{s_\theta(\tilde{y}_2 - \tilde{y}_3)\lambda^5}{\sqrt{2}} & \frac{s_\theta(\tilde{y}_2 + \tilde{y}_3)\lambda^5}{\sqrt{2}} & c_\theta\tilde{y}_1\lambda^3 \end{pmatrix}, \quad (65)$$

hence with off-diagonal elements that vanish in the limit $\theta \rightarrow 0$ it is no longer diagonal in the Z_3 basis of the charged leptons. The perturbed charged lepton mass matrix can be diagonalized to a good approximation by

$$V_L^\dagger M_l V_R = \text{diag}(m_e, m_\mu, m_\tau) \quad (66)$$

with

$$V_R \simeq \begin{pmatrix} 1 & -\frac{\sqrt{2}s_\theta(\tilde{y}_2 - \tilde{y}_3)}{(\tilde{y}_2 + \tilde{y}_3)} & -\frac{\sqrt{2}s_\theta(\tilde{y}_2 - \tilde{y}_3)\lambda^2}{\tilde{y}_1} \\ \frac{\sqrt{2}s_\theta(\tilde{y}_2 - \tilde{y}_3)}{(\tilde{y}_2 + \tilde{y}_3)} & 1 & -\frac{\sqrt{2}s_\theta(\tilde{y}_2 + \tilde{y}_3)\lambda^2}{\tilde{y}_1} \\ \frac{\sqrt{2}s_\theta(\tilde{y}_2 - \tilde{y}_3)\lambda^2}{\tilde{y}_1} & \frac{\sqrt{2}s_\theta(\tilde{y}_2 + \tilde{y}_3)\lambda^2}{\tilde{y}_1} & 1 \end{pmatrix}, \quad (67)$$

$$V_L \simeq U_\omega R O_{23}(\theta) R^T O_{12}(\alpha_L), \quad R = \begin{pmatrix} -\frac{1}{\sqrt{2}} & \frac{1}{\sqrt{2}} & 0 \\ \frac{1}{\sqrt{2}} & \frac{1}{\sqrt{2}} & 0 \\ 0 & 0 & 1 \end{pmatrix},$$

where O_{ij} are rotation matrices in the ij -plane and

$$\tan 2\alpha_L = \frac{s_\theta (4\sqrt{2}c_{3\theta} + 12\sqrt{2}c_\theta - 7s_{3\theta} - 3s_\theta)}{10c_{3\theta} + 6c_\theta + 8\sqrt{2}s_\theta^3}. \quad (68)$$

Using the rotation matrices (Eq. 67)) we find the charged lepton Yukawa couplings $y_{ll'}(l, l' = e, \mu, \tau)$ that eventually lead to flavor violation in the lepton sector. With

$$(\bar{L}_1, \bar{L}_2, \bar{L}_3) = (\bar{L}_e, \bar{L}_\mu, \bar{L}_\tau) V_L^\dagger, \quad (e_1, e_2, e_3)^T = V_R \cdot (e, \mu, \tau)^T, \quad (\phi_1, \phi_2, \phi_3)^T = U_s \cdot (\phi_a, H, h)^T, \quad (69)$$

$$\text{where } U_s \equiv \begin{pmatrix} 0 & \sqrt{\frac{2}{3}} & \frac{1}{\sqrt{3}} \\ -\frac{1}{\sqrt{2}} & -\frac{1}{\sqrt{6}} & \frac{1}{\sqrt{3}} \\ \frac{1}{\sqrt{2}} & -\frac{1}{\sqrt{6}} & \frac{1}{\sqrt{3}} \end{pmatrix} \cdot \begin{pmatrix} 1 & 0 & 0 \\ 0 & c_\theta & -s_\theta \\ 0 & s_\theta & c_\theta \end{pmatrix}, \quad (70)$$

we can identify the coefficients of $h_L l_R'$ as the Yukawas $y_{ll'}$. In leading order, i.e., $m_e \ll m_\mu \ll m_\tau$, the dominant flavor violating couplings are

$$y_{e\tau} \simeq -\frac{m_\tau}{v} (c_{\alpha_L} - s_{\alpha_L}) s_{\vartheta+\theta}, \quad (71)$$

$$y_{\mu\tau} \simeq -\frac{m_\tau}{v} (c_{\alpha_L} + s_{\alpha_L}) s_{\vartheta+\theta}, \quad (72)$$

$$y_{e\mu} \simeq \frac{m_\mu}{4v} (2c_\vartheta (c_{\alpha_L} (c_\theta - 2s_\theta^2 - 1) - s_{\alpha_L} (c_\theta - 2s_\theta^2 + 1)) - s_\vartheta (c_{\alpha_L} (c_\theta (4s_\theta + \sqrt{2}) - 2s_\theta + \sqrt{2}) + s_{\alpha_L} (-c_\theta (4s_\theta + \sqrt{2}) + 2s_\theta + \sqrt{2}))). \quad (73)$$

The remaining off-diagonal couplings are negligibly small and therefore irrelevant for the discussion

$$y_{\tau e} \ll y_{e\tau}, \quad y_{\mu e} \ll y_{e\mu}, \quad y_{\tau\mu} \ll y_{\mu\tau}, \quad (74)$$

which means that $y_{\mu\tau}$ dominates the $h \rightarrow \mu\tau$ decay channel in our model. The perturbation of the VEV alignment has an effect on the PMNS mixing matrix that is negligible for sufficiently small values of θ . This extra contribution modifies the charged lepton contribution to the PMNS mixing matrix as follows

$$V_L = U_\omega W_L \quad \text{with} \quad W_L \simeq \begin{pmatrix} 1 & \frac{\theta}{\sqrt{2}} - \frac{3\theta^2}{4} & \frac{\theta}{\sqrt{2}} \\ -\frac{\theta}{\sqrt{2}} + \frac{3\theta^2}{4} & 1 & \frac{\theta}{\sqrt{2}} \\ -\frac{\theta}{\sqrt{2}} & -\frac{\theta}{\sqrt{2}} & 1 \end{pmatrix}. \quad (75)$$

As we will explain in Sec. III C the values required to explain the $h \rightarrow \mu\tau$ measurement are in the region $|\theta| \lesssim 0.10$ @ 95% C.L. The leptonic mixing angles on the other hand stay within their experimentally determined 3σ ranges for $\theta < 0.08$, but deviations in θ_{12} quickly become too large for increasing values of θ . The full PMNS matrix and the deviations in the mixing angles caused by the perturbation θ are given in Eqs. (D1) and (D2) - (D5) of Appendix D. The breaking of Z_3 also affects the Jarlskog invariant as follows

$$J \approx \frac{\cos(2\psi)}{6\sqrt{3}} + \frac{1}{12}\theta \left(\sqrt{6} \sin(2\psi) \cos(\phi) - \sqrt{2} \sin(2\psi) \sin(\phi) \right) + \frac{1}{24}\theta^2 \left(-3\sqrt{3} \cos(2\psi) - \sin(2\psi) \sin(\phi) + \sqrt{3} \right) \quad (76)$$

and therefore induces CP violation in neutrino oscillations.

By varying ϕ , for $\theta = 0.07$, we obtain the following best-fit result:

$$\text{NH} : \phi = -0.446\pi, \quad \sin^2 \theta_{12} \approx 0.375, \quad \sin^2 \theta_{23} \approx 0.586, \quad \sin^2 \theta_{13} \approx 0.0232, \quad J \approx 1.11 \times 10^{-2}, \quad (77)$$

$$\text{IH} : \phi = 0.553\pi, \quad \sin^2 \theta_{12} \approx 0.375, \quad \sin^2 \theta_{23} \approx 0.588, \quad \sin^2 \theta_{13} \approx 0.0238, \quad J \approx 1.10 \times 10^{-2}. \quad (78)$$

Since the obtained Jarlskog invariant for both NH and IH is approximately 10^{-2} , the Z_3 symmetry breaking can generate a sizeable strength of CP violation in neutrino oscillations for larger θ values.

C. Flavor-violating Higgs decays

As stated in Sec I, the measurement of $h \rightarrow \mu\tau$ is equivalent to a bound on the off-diagonal Yukawa couplings [11]

$$0.0019(0.0008) < \sqrt{|y_{\mu\tau}|^2 + |y_{\tau\mu}|^2} < 0.0032(0.0036) \text{ @ } 68\%(95\%) \text{ C.L.}, \quad (79)$$

where it is assumed that $h \rightarrow \mu\tau$ is the only additional contribution to the SM Higgs decay width. The result in Eq. (79) is well compatible with the current bounds $\text{Br}(\tau \rightarrow \mu\gamma) < 4.4 \times 10^{-8}$ @ 90% C.L. and $\text{Br}(\tau \rightarrow e\gamma) < 3.3 \times 10^{-8}$ @ 90% [32]. However, while small compared to $y_{\mu\tau}$, $y_{e\mu}$ dominates $h \rightarrow e\mu$ and is tightly constrained by $\text{Br}(\mu \rightarrow e\gamma) < 5.7 \times 10^{-13}$ [37], which consequently restricts the allowed values of θ and m_a or m_H . The corresponding diagrams mediating these processes in our model are shown in Fig. 1. Analytically the branching ratio of $l \rightarrow l'\gamma$ is given by [38]

$$\text{Br}(l \rightarrow l'\gamma) = \frac{\tau_l \alpha_{\text{EM}} m_l^5}{64\pi^4} (|c_L|^2 + |c_R|^2), \quad (80)$$

where c_L and c_R are the Wilson coefficients. To calculate c_L and c_R one-loop (cf. Fig. 1) and two-loop contributions are taken into account, where the latter can dominate the branching ratio in certain regions of the parameter space. The full set of equations is shown in Eqs. (E2)-(E11) of Appendix E [38, 39].

Using Eqs. (63), (68) and (71) we determine numerically the allowed values of θ and m_H that can explain the 2.4σ anomaly in $h \rightarrow \mu\tau$ and at the same time respect the bound on $\text{Br}(\mu \rightarrow e\gamma)$, which constraints the $y_{e\mu}$ coupling. Scanning the parameter space for negative and positive values of θ , we find that a window opens up for rather light masses of the extra scalars H and η in the vicinity of the SM Higgs mass, leading to overlap of the regions complying with either $\text{Br}(\mu \rightarrow e\gamma)$ or $\text{Br}(h \rightarrow \mu\tau)$, as shown in Figs. 2a) and 2b). This is where the contributions of the Higgs h to $\text{Br}(\mu \rightarrow e\gamma)$ are partly canceled by the contributions of the neutral scalars H and η , allowing for larger flavor

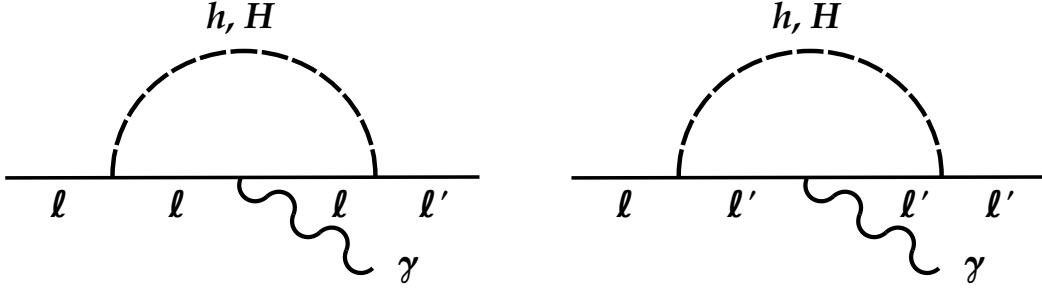


Figure 1: One-Loop diagrams contributing to $l \rightarrow l' \gamma$. Since $|y_u| \gg |y_{l'l'}|$, the left diagram is the dominating one.

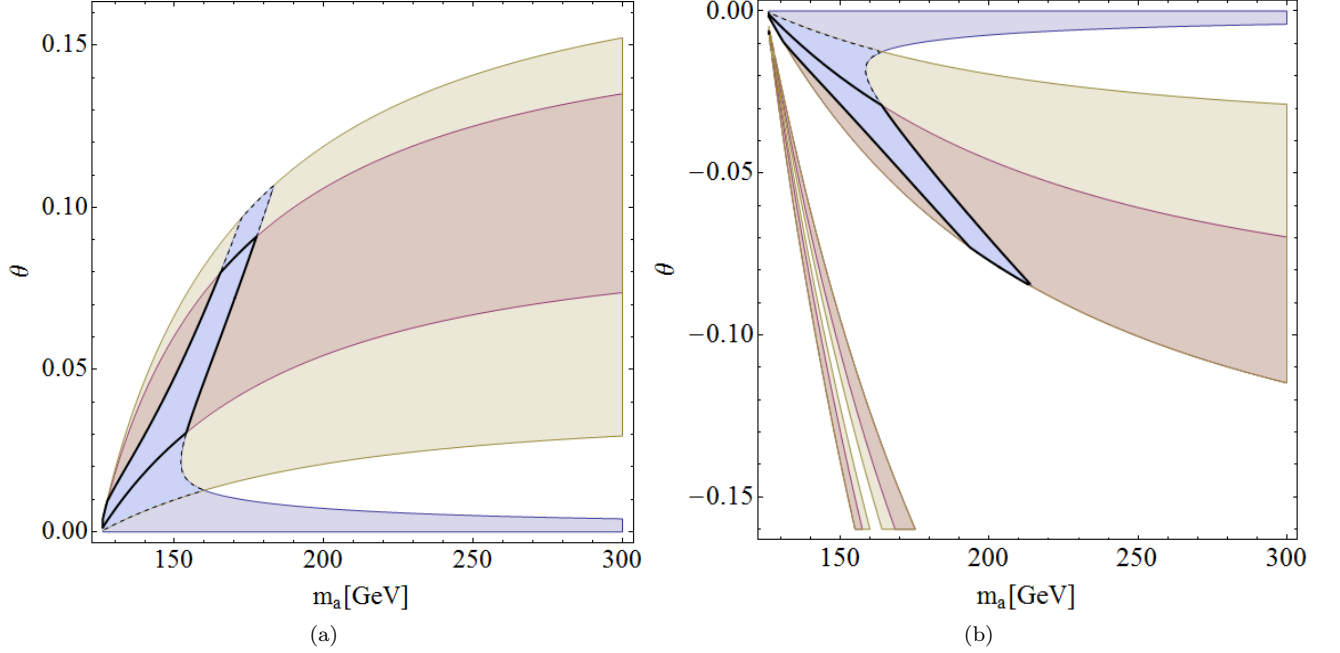


Figure 2: Parameter values leading to $|y_{\mu\tau}|$ required by CMS data on $h \rightarrow \mu\tau$ in brown (68% C.L.) and yellow (95% C.L.) for (a) positive and (b) negative θ . Parameter regions shaded in blue are allowed by $\text{Br}(\mu \rightarrow e\gamma) < 5.7 \times 10^{-13}$. Solid (dashed) lines mark the 1σ (3σ) intervals of $|y_{\mu\tau}|$, where both regions overlap. Overlap occurs for $0.01 \lesssim \theta \lesssim 0.09$, $126 \text{ GeV} \lesssim m_H \lesssim 204 \text{ GeV}$ (68% C.L.) and $-0.08 \lesssim \theta \lesssim -0.01$, $127 \text{ GeV} \lesssim m_H \lesssim 190 \text{ GeV}$ (68% C.L.) allowing us to explain the excess in $h \rightarrow \mu\tau$ and at the same time to comply with the tight bound on $\text{Br}(\mu \rightarrow e\gamma)$ ($m_\eta = 200 \text{ GeV}$).

violating Yukawa couplings in these regions. The parameter space is practically symmetric around $\theta = 0$, i.e., at 68% C.L.(95% C.L.) and $m_\eta = 200 \text{ GeV}$

$$\begin{aligned} 0.002 (0.001) < \theta < 0.090 (0.104), & 126 (126) \text{ GeV} < m_H < 204 (214) \text{ GeV}, \\ -0.004 (-0.001) > \theta > -0.082 (-0.082), & 127 (126) \text{ GeV} < m_H < 190 (190) \text{ GeV}. \end{aligned} \quad (81)$$

Using the determined 1σ parameter ranges (Eq. (81)), we can also make other predictions for rare decays, where by far the strongest constraints come from the radiative decays $l \rightarrow l' \gamma$. The flavor violating modes $\text{Br}(\tau \rightarrow 3\mu) < 2.1 \times 10^{-8}$, $\text{Br}(\tau \rightarrow 3e) < 2.7 \times 10^{-8}$ and $\text{Br}(\mu \rightarrow 3e) < 1.0 \times 10^{-12}$ [32] are approximately

$$\text{Br}(l \rightarrow 3l') = -\frac{\tau_l \alpha_{\text{EM}}^2 m_l^5}{72(2\pi)^5} \left[12 \log \frac{m_l'^2}{m_l^2} + 29 + 6 \log 4 \right] (|c_L|^2 + |c_R|^2), \quad (82)$$

assuming that loop diagrams in the spirit of Fig. 1 (γ decays into $l^+ l^-$) dominate over the tree level exchange of a neutral scalar field [38].

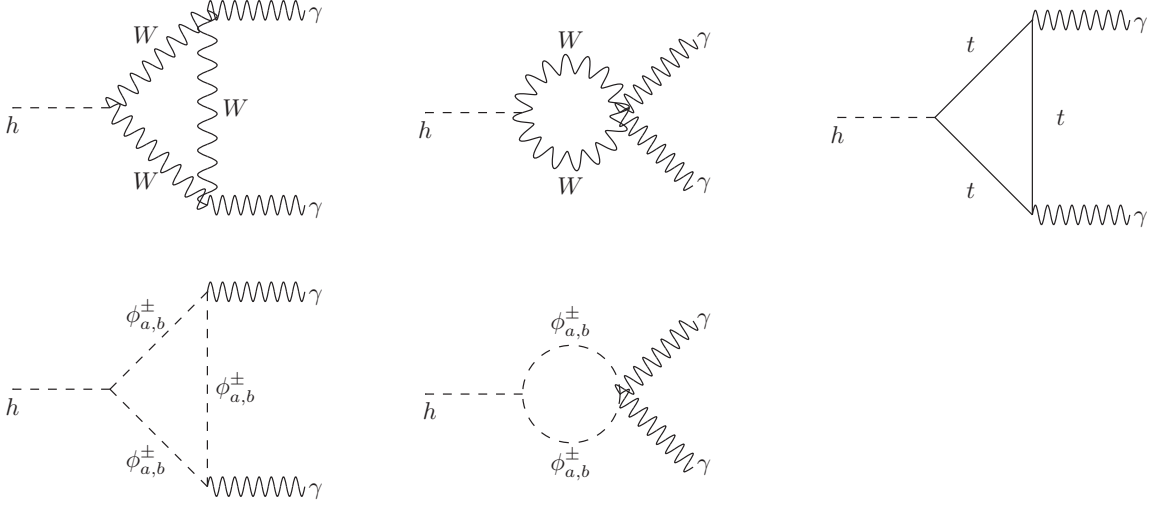


Figure 3: One-loop Feynman diagrams in the unitary gauge contributing to the $h \rightarrow \gamma\gamma$ decay.

Our predictions for $0.01 \lesssim \theta \lesssim 0.09$, $126 \text{ GeV} \lesssim m_H \lesssim 204 \text{ GeV}$ ($m_\eta = 200 \text{ GeV}$),

$$\begin{aligned}
 \text{Br}(\tau \rightarrow \mu\gamma) &\in (0.3 - 1.3) \times 10^{-8}, & \text{Br}(\tau \rightarrow e\gamma) &\in (0.3 - 1.3) \times 10^{-8}, \\
 \text{Br}(\tau \rightarrow 3\mu) &\in (1.9 - 8.1) \times 10^{-10}, & \text{Br}(\tau \rightarrow 3e) &\in (0.9 - 4.1) \times 10^{-9}, \\
 \text{Br}(h \rightarrow e\tau) &\in (0.4 - 1.2) \times 10^{-2}, & \text{Br}(h \rightarrow e\mu) &\in (1.5 - 4.2) \times 10^{-5},
 \end{aligned} \tag{83}$$

and $-0.08 \lesssim \theta \lesssim -0.01$, $127 \text{ GeV} \lesssim m_H \lesssim 190 \text{ GeV}$,

$$\begin{aligned}
 \text{Br}(\tau \rightarrow \mu\gamma) &\in (0.3 - 1.2) \times 10^{-8}, & \text{Br}(\tau \rightarrow e\gamma) &\in (0.3 - 1.2) \times 10^{-8}, \\
 \text{Br}(\tau \rightarrow 3\mu) &\in (2.0 - 7.6) \times 10^{-10}, & \text{Br}(\tau \rightarrow 3e) &\in (1.1 - 4.1) \times 10^{-9}, \\
 \text{Br}(h \rightarrow e\tau) &\in (0.5 - 1.4) \times 10^{-2}, & \text{Br}(h \rightarrow e\mu) &\in (1.5 - 4.1) \times 10^{-5},
 \end{aligned} \tag{84}$$

are throughout below the current bounds in these particular parameter regions, but not too small to be out of reach for future experiments. A measurement of the $h \rightarrow e\tau$ channel using the newest LHC data should be the fastest way to rule out this model in the near future, as our prediction for this channel is unambiguously connected to $h \rightarrow \mu\tau$ and expected to be the same order of magnitude,

$$\frac{\text{Br}(h \rightarrow \mu\tau)}{\text{Br}(h \rightarrow e\tau)} \approx \frac{|y_{\mu\tau}|^2}{|y_{e\tau}|^2} \approx \frac{(c_{\alpha_L} + s_{\alpha_L})^2}{(c_{\alpha_L} - s_{\alpha_L})^2},$$

which is approximately 1 for small values of θ . Using Eqs. (30) and (76), we also predict a nonvanishing leptonic CP phase $\delta_{CP}^L \approx 0.3$ at $\theta = 0.07$, the maximal value still in agreement with the lepton mixing angle θ_{12} .

IV. CONSTRAINTS FROM $h \rightarrow \gamma\gamma$

As shown in the previous section, small Z_3 breaking perturbations allow to successfully accommodate the experimental CMS data on the $h \rightarrow \mu\tau$ excess. Consequently and in order to make definite predictions, it is reasonable to neglect these perturbations in the computation of the Higgs diphoton decay rate. In the SM, the $h \rightarrow \gamma\gamma$ decay is dominated by W -loop diagrams which can interfere destructively with the subdominant top quark loop. In our 3HDM, the $h \rightarrow \gamma\gamma$ decay receives additional contributions from loops with charged scalars $\phi_{(a,b)}^\pm$, as shown in Fig. 3, and therefore sets bounds on the masses of these scalars.

The explicit form of the $h \rightarrow \gamma\gamma$ decay rate is [40–45]

$$\Gamma(h \rightarrow \gamma\gamma) = \frac{\alpha_{em}^2 m_h^3}{256\pi^3 v^2} \left| \sum_f a_{hff} N_C Q_f^2 F_{1/2}(\beta_f) + F_1(\beta_W) + \sum_{s=a,b} \frac{\lambda_{h\phi_s^\pm \phi_s^\mp} v}{2m_{\phi_s^\pm}^2} F_0(\beta_{\phi_s^\pm}) \right|^2 \quad (85)$$

Here β_i are the mass ratios $\beta_i = \frac{m_h^2}{4M_i^2}$, with $M_i = m_f, M_W$, and $m_{\phi_{a,b}^\pm}$, α_{em} is the fine structure constant, N_C is the color factor ($N_C = 1$ for leptons, $N_C = 3$ for quarks), and Q_f is the electric charge of the fermion in the loop. From the fermion-loop contributions we consider only the dominant top quark term. Furthermore, $\lambda_{h\phi_s^\pm \phi_s^\mp}$ is the trilinear coupling between the SM-like Higgs and a pair of charged Higgses, which in the case of an exact Z_3 symmetry is given by

$$\lambda_{h\phi_s^\pm \phi_s^\mp} = \frac{2}{3} (3\alpha + 2\beta - \gamma - \delta) v = \frac{2(m_h^2 - m_{\phi_s^\pm}^2)}{v}, \quad s = a, b. \quad (86)$$

The dimensionless loop factors $F_{1/2}(\beta)$ and $F_1(\beta)$ can be found in Eqs. (F1) - (F4) of Appendix F.

In what follows we determine the range of values for the charged Higgs boson masses $m_{\phi_{a,b}^\pm}$ which are consistent with the $h \rightarrow \gamma\gamma$ results at the LHC. To this end, we introduce the ratio $R_{\gamma\gamma}$, which normalizes the $\gamma\gamma$ signal predicted by our model relative to that of the SM:

$$R_{\gamma\gamma} = \frac{\sigma(pp \rightarrow h) \Gamma(h \rightarrow \gamma\gamma)}{\sigma(pp \rightarrow h)_{SM} \Gamma(h \rightarrow \gamma\gamma)_{SM}} \simeq a_{htt}^2 \frac{\Gamma(h \rightarrow \gamma\gamma)}{\Gamma(h \rightarrow \gamma\gamma)_{SM}}, \quad (87)$$

where a_{htt} is the deviation of the Higgs-top quark coupling with respect to the SM. Here we set a_{htt} to be equal to one as in the SM based on the fact that in our model single Higgs production is also dominated by gluon fusion. The normalization given by Eq. (87) for $h \rightarrow \gamma\gamma$ was also used in Refs. [46–48].

The ratio $R_{\gamma\gamma}$ has been measured by CMS and ATLAS with the best-fit signals [49, 50]

$$R_{\gamma\gamma}^{\text{CMS}} = 1.14_{-0.23}^{+0.26} \quad \text{and} \quad R_{\gamma\gamma}^{\text{ATLAS}} = 1.17 \pm 0.27, \quad (88)$$

which are used to limit the charged scalar masses contributing to $h \rightarrow \gamma\gamma$. Figure 4 shows the sensitivity of the ratio $R_{\gamma\gamma}$ under variations of the charged Higgs masses $m_{\phi_s^\pm}$ ($s = a, b$), between 200 GeV and 1 TeV. We consider charged Higgs boson masses larger than 200 GeV to ensure they are in the region above the $W^\pm h$ threshold, as done in Ref [51]. The ratio $R_{\gamma\gamma}$ slowly increases when the charged Higgs boson masses are increased. Requiring that the $h \rightarrow \gamma\gamma$ signal stays within the range $1.14 \lesssim R_{\gamma\gamma} \lesssim 1.17$ (the central values of the recent CMS and ATLAS results, respectively), yields the bound $200 \text{ GeV} \lesssim m_{\phi_{a,b}^\pm} \lesssim 205 \text{ GeV}$ for the charged Higgs boson masses. However, considering the experimental errors of the measurements, the parameter space consistent with the Higgs diphoton signal becomes larger, i.e., masses in the range $200 \text{ GeV} \lesssim m_{\phi_{a,b}^\pm} \lesssim 1 \text{ TeV}$ can successfully account for the $h \rightarrow \gamma\gamma$ rate observed at the LHC. The scalar sector can be constrained further from the analysis of the T and S parameters, for details see Appendix B.

V. CONCLUSIONS

In summary we have presented a 3HDM with LFT, where strongly constrained FCNCs are suppressed by virtue of a residual Z_3 symmetry. A small breaking of the Z_3 symmetry can give rise to LFV Higgs decays, occurring naturally in our model due to $SU(2)$ singlet scalars in the scalar potential. Furthermore, a small breaking of the Z_3 symmetry also gives rise to CP violation in neutrino oscillations. We obtain a sizable branching ratio particularly in the flavor violating $h \rightarrow \mu^e \tau$ channel, accounting for the 2.4σ deviation from the SM as indicated by recent CMS results. This is a consequence of mixing between an SM-like Higgs with a nonstandard neutral scalar that can decay into flavor violating final states. If the extra neutral scalars are light, they can partly cancel Higgs loop contributions to $l \rightarrow l' \gamma$, allowing for large flavor violating Yukawa couplings. We thus also expect large branching fractions for $h \rightarrow e\mu$ and $h \rightarrow e\tau$ in our model, where the latter will be a decisive measurement for its exclusion. Furthermore, the $h \rightarrow \gamma\gamma$ rate measured by ATLAS and CMS favors charged Higgs boson masses of less than 205 GeV, but the large experimental uncertainties still allow for masses of up to 1 TeV in our model.

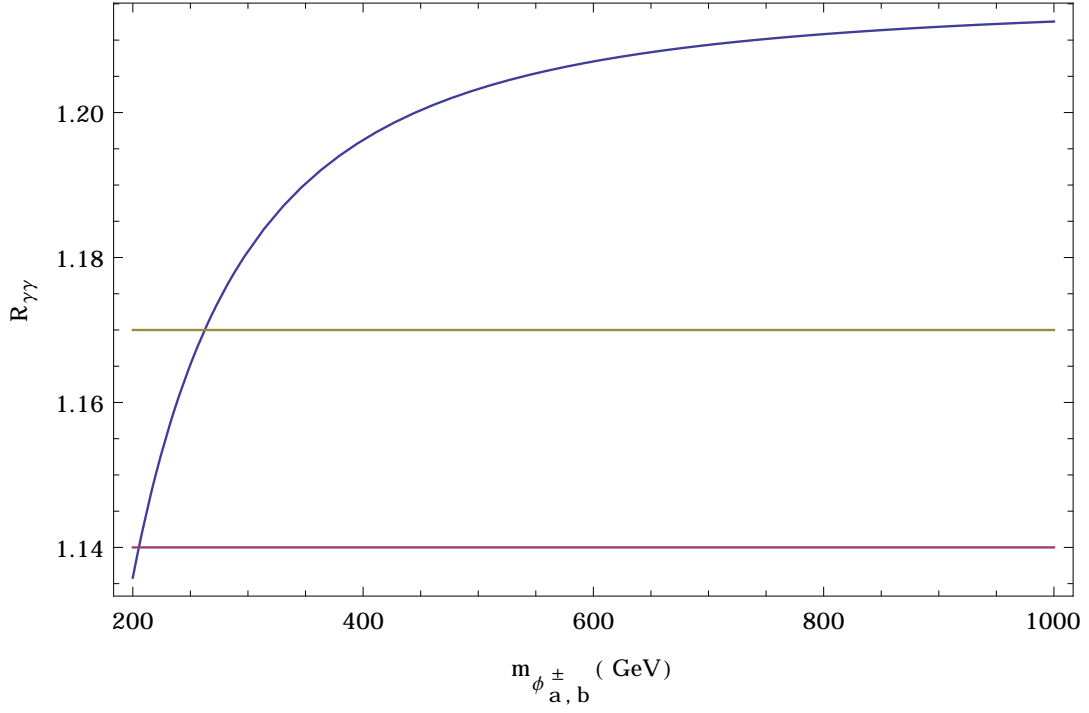


Figure 4: The ratio $R_{\gamma\gamma}$ as a function of the charged Higgs masses $m_{\phi_s^\pm}$ ($s = a, b$) for $a_{htt} = 1$. The horizontal lines are the $R_{\gamma\gamma}$ experimental values given by CMS and ATLAS, which are equal to $1.14^{+0.26}_{-0.23}$ and 1.17 ± 0.27 , respectively [49, 50].

Acknowledgments

We thank Gautam Bhattacharyya and Ivo de Medeiros Varzielas for useful discussions. A.E.C.H thanks the TU Dortmund for hospitality and for partially financing his visit. A.E.C.H was partially supported by Fondecyt (Chile), Grant No. 11130115 and by DGIP internal Grant No. 111458. M.D.C. thanks the DAAD for supporting his visit to the TU Dortmund.

Appendix A: S_4 Symmetry

S_4 , the group of permutations of four objects, contains five irreducible representations $\mathbf{1}, \mathbf{1}', \mathbf{2}, \mathbf{3}, \mathbf{3}'$ obeying the following tensor product rules [52]:

$$\mathbf{3} \otimes \mathbf{3} = \mathbf{1} \oplus \mathbf{2} \oplus \mathbf{3} \oplus \mathbf{3}', \quad \mathbf{3}' \otimes \mathbf{3}' = \mathbf{1} \oplus \mathbf{2} \oplus \mathbf{3} \oplus \mathbf{3}', \quad \mathbf{3} \otimes \mathbf{3}' = \mathbf{1}' \oplus \mathbf{2} \oplus \mathbf{3} \oplus \mathbf{3}', \quad (\text{A1})$$

$$\mathbf{2} \otimes \mathbf{2} = \mathbf{1} \oplus \mathbf{1}' \oplus \mathbf{2}, \quad \mathbf{2} \otimes \mathbf{3} = \mathbf{3} \oplus \mathbf{3}', \quad \mathbf{2} \otimes \mathbf{3}' = \mathbf{3}' \oplus \mathbf{3}, \quad (\text{A2})$$

$$\mathbf{3} \otimes \mathbf{1}' = \mathbf{3}', \quad \mathbf{3}' \otimes \mathbf{1}' = \mathbf{3}, \quad \mathbf{2} \otimes \mathbf{1}' = \mathbf{2}. \quad (\text{A3})$$

Explicitly, the basis used in this paper corresponds to Ref. [52] and results in

$$(\mathbf{A})_{\mathbf{3}} \times (\mathbf{B})_{\mathbf{3}} = (\mathbf{A} \cdot \mathbf{B})_{\mathbf{1}} + \begin{pmatrix} \mathbf{A} \cdot \Sigma \cdot \mathbf{B} \\ \mathbf{A} \cdot \Sigma^* \cdot \mathbf{B} \end{pmatrix}_{\mathbf{2}} + \begin{pmatrix} \{A_y B_z\} \\ \{A_z B_x\} \\ \{A_x B_y\} \end{pmatrix}_{\mathbf{3}} + \begin{pmatrix} [A_y B_z] \\ [A_z B_x] \\ [A_x B_y] \end{pmatrix}_{\mathbf{3}'}, \quad (\text{A4})$$

$$(\mathbf{A})_{\mathbf{3}'} \times (\mathbf{B})_{\mathbf{3}'} = (\mathbf{A} \cdot \mathbf{B})_{\mathbf{1}} + \begin{pmatrix} \mathbf{A} \cdot \Sigma \cdot \mathbf{B} \\ \mathbf{A} \cdot \Sigma^* \cdot \mathbf{B} \end{pmatrix}_{\mathbf{2}} + \begin{pmatrix} \{A_y B_z\} \\ \{A_z B_x\} \\ \{A_x B_y\} \end{pmatrix}_{\mathbf{3}} + \begin{pmatrix} [A_y B_z] \\ [A_z B_x] \\ [A_x B_y] \end{pmatrix}_{\mathbf{3}'}, \quad (\text{A5})$$

$$(\mathbf{A})_{\mathbf{3}} \times (\mathbf{B})_{\mathbf{3}'} = (\mathbf{A} \cdot \mathbf{B})_{\mathbf{1}'} + \begin{pmatrix} \mathbf{A} \cdot \Sigma \cdot \mathbf{B} \\ -\mathbf{A} \cdot \Sigma^* \cdot \mathbf{B} \end{pmatrix}_{\mathbf{2}} + \begin{pmatrix} \{A_y B_z\} \\ \{A_z B_x\} \\ \{A_x B_y\} \end{pmatrix}_{\mathbf{3}'} + \begin{pmatrix} [A_y B_z] \\ [A_z B_x] \\ [A_x B_y] \end{pmatrix}_{\mathbf{3}}, \quad (\text{A6})$$

$$(\mathbf{A})_{\mathbf{2}} \times (\mathbf{B})_{\mathbf{2}} = \{A_x B_y\}_{\mathbf{1}} + [A_x B_y]_{\mathbf{1}'} + \begin{pmatrix} A_y B_y \\ A_x B_x \end{pmatrix}_{\mathbf{2}}, \quad (\text{A7})$$

$$\begin{pmatrix} A_x \\ A_y \end{pmatrix}_{\mathbf{2}} \times \begin{pmatrix} B_x \\ B_y \\ B_z \end{pmatrix}_{\mathbf{3}} = \begin{pmatrix} (A_x + A_y)B_x \\ (\omega^2 A_x + \omega A_y)B_y \\ (\omega A_x + \omega^2 A_y)B_z \end{pmatrix}_{\mathbf{3}} + \begin{pmatrix} (A_x - A_y)B_x \\ (\omega^2 A_x - \omega A_y)B_y \\ (\omega A_x - \omega^2 A_y)B_z \end{pmatrix}_{\mathbf{3}'}, \quad (\text{A8})$$

$$\begin{pmatrix} A_x \\ A_y \end{pmatrix}_{\mathbf{2}} \times \begin{pmatrix} B_x \\ B_y \\ B_z \end{pmatrix}_{\mathbf{3}'} = \begin{pmatrix} (A_x + A_y)B_x \\ (\omega^2 A_x + \omega A_y)B_y \\ (\omega A_x + \omega^2 A_y)B_z \end{pmatrix}_{\mathbf{3}'} + \begin{pmatrix} (A_x - A_y)B_x \\ (\omega^2 A_x - \omega A_y)B_y \\ (\omega A_x - \omega^2 A_y)B_z \end{pmatrix}_{\mathbf{3}}, \quad (\text{A9})$$

with

$$\mathbf{A} \cdot \mathbf{B} = A_x B_x + A_y B_y + A_z B_z, \quad (\text{A10})$$

$$\{A_x B_y\} = A_x B_y + A_y B_x, \quad (\text{A11})$$

$$[A_x B_y] = A_x B_y - A_y B_x, \quad (\text{A12})$$

$$\mathbf{A} \cdot \Sigma \cdot \mathbf{B} = A_x B_x + \omega A_y B_y + \omega^2 A_z B_z, \quad (\text{A13})$$

$$\mathbf{A} \cdot \Sigma^* \cdot \mathbf{B} = A_x B_x + \omega^2 A_y B_y + \omega A_z B_z, \quad (\text{A14})$$

where $\omega = e^{2\pi i/3}$ is a complex square root of unity.

Appendix B: T and S parameter constraints

The inclusion of the extra scalar particles modifies the oblique corrections of the SM, the values which have been extracted from high precision experiments. Consequently, the validity of the different flavor models that we are

considering depends on the condition that the extra particles do not contradict those experimental results. These oblique corrections are parametrized in terms of the two well-known quantities T and S . The T parameter is defined as [53–56]:

$$T = \frac{\Pi_{33}(0) - \Pi_{11}(0)}{M_W^2 \alpha_{em}(m_Z)}. \quad (\text{B1})$$

where $\Pi_{11}(0)$ and $\Pi_{33}(0)$ are the vacuum polarization amplitudes at $q^2 = 0$ for loop diagrams having gauge bosons W_μ^1 , W_μ^1 and W_μ^3 , W_μ^3 in the external lines, respectively. In turn, the S parameter is defined by [53–56]:

$$S = \frac{4 \sin^2 \theta_W}{\alpha_{em}(m_Z)} \frac{g}{g'} \left. \frac{d\Pi_{30}(q^2)}{dq^2} \right|_{q^2=0}, \quad (\text{B2})$$

where $\Pi_{30}(q^2)$ is the vacuum polarization amplitude for a loop diagram having W_μ^3 and B_μ in the external lines. The Feynman diagrams contributing to the T and S parameters are shown in Figs. 5 and 6.

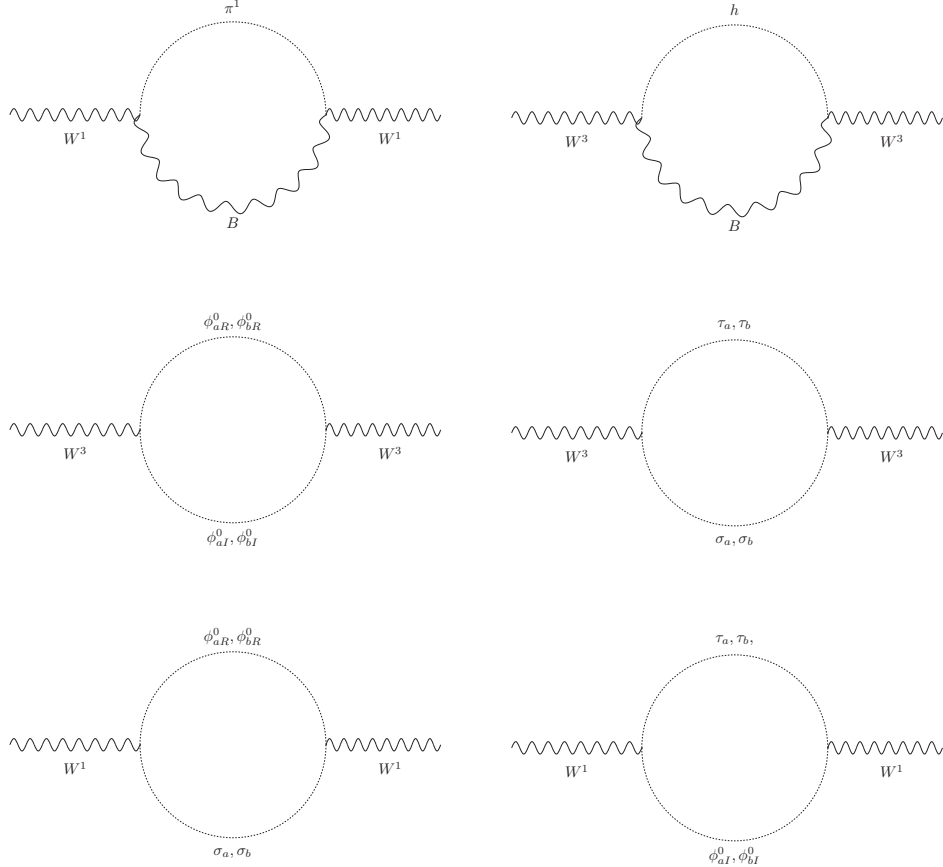
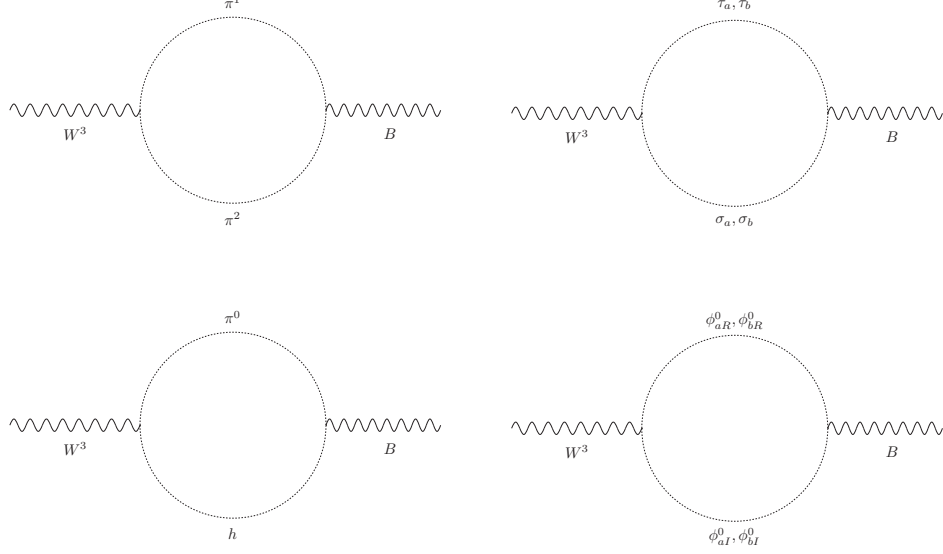


Figure 5: One-loop Feynman diagrams contributing to the T parameter.

We can split the T and S parameters as $T = T_{SM} + \Delta T$ and $S = S_{SM} + \Delta S$, where T_{SM} and S_{SM} are the contributions from the SM, while ΔT and ΔS contain all the contributions involving the extra particles

$$T_{SM} = -\frac{3}{16\pi \cos^2 \theta_W} \ln \left(\frac{m_h^2}{m_W^2} \right), \quad S_{SM} = \frac{1}{12\pi} \ln \left(\frac{m_h^2}{m_W^2} \right) \quad (\text{B3})$$

Figure 6: One-loop Feynman diagrams contributing to the S parameter.

$$\Delta T \simeq \frac{1}{16\pi^2 v^2 \alpha_{em}(m_Z)} \sum_{f=a,b} \left[m_{\phi_f^\pm}^2 - H(m_{\phi_{fI}^0}^2, m_{\phi_f^\pm}^2) + H(m_{\phi_{fR}^0}^2, m_{\phi_{fI}^0}^2) - H(m_{\phi_{fR}^0}^2, m_{\phi_f^\pm}^2) \right] \quad (\text{B4})$$

$$\Delta S \simeq \frac{1}{12\pi} \sum_{f=a,b} K(m_{\phi_{fR}^0}^2, m_{\phi_{fI}^0}^2, m_{\phi_f^\pm}^2), \quad (\text{B5})$$

where we introduced the following functions [57]:

$$H(m_1^2, m_2^2) = \frac{m_1^2 m_2^2}{m_1^2 - m_2^2} \ln \left(\frac{m_1^2}{m_2^2} \right), \quad \lim_{m_2 \rightarrow m_1} H(m_1^2, m_2^2) = m_1^2. \quad (\text{B6})$$

$$K(m_1^2, m_2^2, m_3^2) = \frac{1}{(m_2^2 - m_1^2)^3} \left\{ m_1^4 (3m_2^2 - m_1^2) \ln \left(\frac{m_1^2}{m_3^2} \right) - m_2^4 (3m_1^2 - m_2^2) \ln \left(\frac{m_2^2}{m_3^2} \right) - \frac{1}{6} [27m_1^2 m_2^2 (m_1^2 - m_2^2) + 5(m_2^6 - m_1^6)] \right\}. \quad (\text{B7})$$

The experimental results on T and S restrict ΔT and ΔS to lie inside a region in the $\Delta S - \Delta T$ plane. At the 95% C.L. (confidence level), these regions are the elliptic contours shown in Fig. 7. The origin $\Delta S = \Delta T = 0$ corresponds to the SM value, with $m_h = 125.5$ GeV and $m_t = 176$ GeV. One can consider a scenario in which the heavy neutral CP-even and neutral CP-odd scalars are degenerate. For a mass of $m_{\phi_{(a,b)I}^0} = m_{\phi_{(a,b)R}^0} = 130$ GeV, consistency with the T and S parameters confines the masses of the charged scalars to $130 \text{ GeV} \leq m_{\phi_{(a,b)}^\pm} \leq 196$ GeV, whereas for $m_{\phi_{(a,b)I}^0} = m_{\phi_{(a,b)R}^0} = 600$ GeV, the charged scalar masses are in the range $600 \text{ GeV} \leq m_{\phi_{(a,b)}^\pm} \leq 672$ GeV while for $m_{\phi_{(a,b)I}^0} = m_{\phi_{(a,b)R}^0} = 1$ TeV, the masses of the charged scalars range between 925 and 990 GeV. In Figs. 7(a)-7(c) we show the allowed regions for the ΔT and ΔS parameters, for the three sets of values of $m_{\phi_{(a,b)I}^0}$ and $m_{\phi_{(a,b)R}^0}$ previously indicated. The line going upwards inside the ellipses corresponds to the several $(\Delta S, \Delta T)$ points of the model when the charged scalar masses are varied inside the interval previously specified.

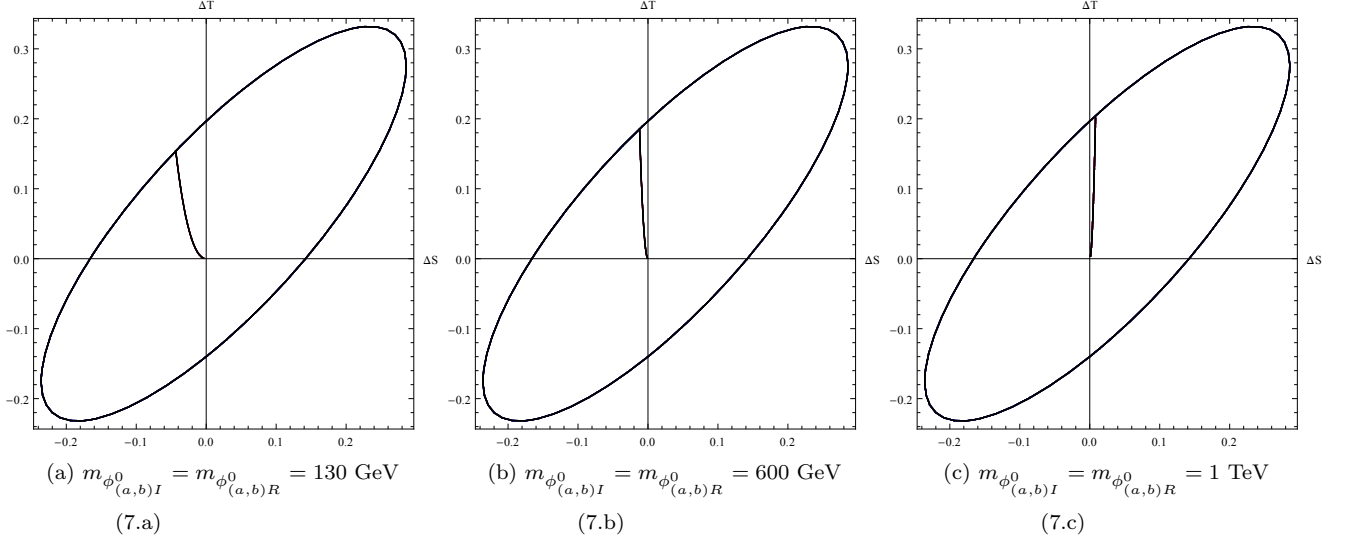


Figure 7: The $\Delta S - \Delta T$ plane, where the ellipses denote the experimentally allowed region at 95% C.L. taken from [58–60]. The origin $\Delta S = \Delta T = 0$ corresponds to the SM value, with $m_h = 125.5 \text{ GeV}$ and $m_t = 176 \text{ GeV}$. Figures (a), (b) and (c) correspond to two different sets of values for the masses of the neutral non-SM Higgs bosons, as indicated. The mass $m_{\phi_{(a,b)}^\pm}$ of the charged Higgs bosons varies between $130 \text{ GeV} \leq m_{\phi_{(a,b)}^\pm} \leq 196 \text{ GeV}$ (Fig. 7(a)), $600 \text{ GeV} \leq m_{\phi_{(a,b)}^\pm} \leq 672 \text{ GeV}$ (Fig. 7(b)), $925 \text{ GeV} \leq m_{\phi_{(a,b)}^\pm} \leq 990 \text{ GeV}$ (Fig. 7(c)). The lines originating in the center of the plot and running up towards the ellipses correspond to the obtained values of the ΔT and ΔS parameters in our model, as the charged Higgs boson masses are varied in the aforementioned ranges.

Appendix C: Quark masses and mixings

The relevant $S_4 \otimes Z_2'' \otimes Z_6 \otimes Z_{12}$ -invariant Yukawa terms for the up-type quark sector are

$$\begin{aligned}
 \mathcal{L}^{(U)} = & y_1^{(t)} [Q\phi]_{3'} t_R \frac{\rho}{\Lambda} + \frac{y_2^{(t)}}{\Lambda} Q [\phi\rho]_{3'} t_R + y_3^{(t)} [Q\phi]_{3'} t_R \frac{\rho}{\Lambda} + \frac{y_4^{(t)}}{\Lambda} Q [\phi\rho]_{3'} t_R \\
 & + x_1^{(t)} [Q\phi]_3 t_R \frac{\varphi}{\Lambda} + \frac{x_2^{(t)}}{\Lambda} Q [\phi\varphi]_{3'} t_R + x_3^{(t)} [Q\phi]_3 t_R \frac{\varphi}{\Lambda} + \frac{x_4^{(t)}}{\Lambda} Q [\phi\varphi]_{3'} t_R \\
 & + y_1^{(c)} [Q\phi]_{3'} c_R \frac{\rho}{\Lambda} + \frac{y_2^{(c)}}{\Lambda} Q [\phi\rho]_{3'} c_R + y_3^{(c)} [Q\phi]_{3'} c_R \frac{\rho}{\Lambda} + \frac{y_4^{(c)}}{\Lambda} Q [\phi\rho]_{3'} c_R \\
 & + x_1^{(c)} [Q\phi]_3 c_R \frac{\varphi}{\Lambda} + \frac{x_2^{(c)}}{\Lambda} Q [\phi\varphi]_{3'} c_R + x_3^{(c)} [Q\phi]_3 c_R \frac{\varphi}{\Lambda} + \frac{x_4^{(c)}}{\Lambda} Q [\phi\varphi]_{3'} c_R + x_0^{(u)} [Q\phi]_1 u_R \frac{\Omega_2^3}{\Lambda^3} \\
 & + y_1^{(u)} [Q\phi]_{3'} u_R \frac{\rho\Omega_1^2}{\Lambda^3} + y_2^{(u)} Q [\phi\rho]_{3'} u_R \frac{\Omega_1^2}{\Lambda^3} + y_3^{(u)} [Q\phi]_{3'} u_R \frac{\rho\Omega_1^2}{\Lambda^4} + \frac{y_4^{(u)}}{\Lambda} Q [\phi\rho]_{3'} u_R \frac{\Omega_1^2}{\Lambda^3} \\
 & + x_1^{(u)} [Q\phi]_{3'} u_R \frac{\varphi\Omega_1^2}{\Lambda^3} + x_2^{(u)} Q [\phi\varphi]_{3'} u_R \frac{\Omega_1^2}{\Lambda^3} + x_3^{(c)} [Q\phi]_3 u_R \frac{\varphi}{\Lambda} + \frac{x_4^{(c)}}{\Lambda} Q [\phi\varphi]_{3'} u_R \frac{\Omega_1^2}{\Lambda^3}
 \end{aligned} \tag{C1}$$

and for the down-type quarks

$$\begin{aligned}
\mathcal{L}_1^{(D)} = & y_1^{(b)} [Q\phi]_{3'} b_R \frac{\rho\Omega_3^3}{\Lambda^4} + \frac{y_2^{(b)}}{\Lambda} Q [\phi\rho]_{3'} b_R \frac{\Omega_3^3}{\Lambda^3} + y_3^{(b)} [Q\phi]_{3'} b_R \frac{\rho\Omega_3^3}{\Lambda^4} + \frac{y_4^{(b)}}{\Lambda} Q [\phi\rho]_{3'} b_R \frac{\Omega_3^3}{\Lambda^3} \\
& + x_1^{(b)} [Q\phi]_3 b_R \frac{\varphi\Omega_3^3}{\Lambda^4} + \frac{x_2^{(b)}}{\Lambda} Q [\phi\varphi]_{3'} b_R \frac{\Omega_3^3}{\Lambda^3} + x_3^{(b)} [Q\phi]_3 b_R \frac{\varphi\Omega_3^3}{\Lambda^4} + \frac{x_4^{(b)}}{\Lambda} Q [\phi\varphi]_{3'} b_R \frac{\Omega_3^3}{\Lambda^3} \\
& + y_1^{(s)} [Q\phi]_{3'} s_R \frac{\rho\Omega_3^3}{\Lambda^4} + \frac{y_2^{(b)}}{\Lambda} Q [\phi\rho]_{3'} s_R \frac{\Omega_3^3}{\Lambda^3} + y_3^{(b)} [Q\phi]_{3'} s_R \frac{\rho\Omega_3^3}{\Lambda^4} + \frac{y_4^{(b)}}{\Lambda} Q [\phi\rho]_{3'} s_R \frac{\Omega_3^3}{\Lambda^3} \\
& + x_1^{(s)} [Q\phi]_3 s_R \frac{\varphi\Omega_3^3}{\Lambda^4} + \frac{x_2^{(s)}}{\Lambda} Q [\phi\varphi]_{3'} s_R \frac{\Omega_3^3}{\Lambda^3} + x_3^{(s)} [Q\phi]_3 s_R \frac{\varphi\Omega_3^3}{\Lambda^4} + \frac{x_4^{(s)}}{\Lambda} Q [\phi\varphi]_{3'} s_R \frac{\Omega_3^3}{\Lambda^3} \\
& + x_0^{(d)} [Q\phi]_1 d_R \frac{\Omega_2^2\Omega_3^3}{\Lambda^5} + y_1^{(d)} [Q\phi]_{3'} d_R \frac{\rho\Omega_1\Omega_3^3}{\Lambda^5} + y_2^{(d)} Q [\phi\rho]_{3'} d_R \frac{\Omega_1\Omega_3^3}{\Lambda^5} + y_3^{(d)} [Q\phi]_{3'} d_R \frac{\rho\Omega_1\Omega_3^3}{\Lambda^5} \\
& + \frac{y_4^{(d)}}{\Lambda} Q [\phi\rho]_{3'} d_R \frac{\Omega_1\Omega_3^3}{\Lambda^5} + x_1^{(d)} [Q\phi]_{3'} d_R \frac{\varphi\Omega_1\Omega_3^3}{\Lambda^5} + x_2^{(d)} Q [\phi\varphi]_{3'} d_R \frac{\Omega_1\Omega_3^3}{\Lambda^5} \\
& + x_3^{(d)} [Q\phi]_3 d_R \frac{\varphi\Omega_3^3}{\Lambda^5} + x_4^{(d)} Q [\phi\varphi]_{3'} d_R \frac{\Omega_1\Omega_3^3}{\Lambda^5}.
\end{aligned} \tag{C2}$$

Appendix D: PMNS matrix after Z_3 breaking

The PMNS matrix receives corrections caused by the perturbation of the VEV alignment. These are approximately given by

$$\begin{aligned}
U \simeq & \begin{pmatrix} \frac{\cos\psi}{\sqrt{3}} - \frac{e^{i\phi-\frac{2i\pi}{3}}\sin\psi}{\sqrt{3}} & \frac{e^{\frac{2i\pi}{3}}}{\sqrt{3}} & \frac{e^{-\frac{2i\pi}{3}}\cos\psi}{\sqrt{3}} + \frac{e^{-i\phi}\sin\psi}{\sqrt{3}} \\ \frac{\cos\psi}{\sqrt{3}} - \frac{e^{i\phi+\frac{2i\pi}{3}}\sin\psi}{\sqrt{3}} & \frac{e^{-\frac{2i\pi}{3}}}{\sqrt{3}} & \frac{e^{\frac{2i\pi}{3}}\cos\psi}{\sqrt{3}} + \frac{e^{-i\phi}\sin\psi}{\sqrt{3}} \\ \frac{\cos\psi}{\sqrt{3}} - \frac{e^{i\phi}\sin\psi}{\sqrt{3}} & \frac{1}{\sqrt{3}} & \frac{\cos\psi}{\sqrt{3}} + \frac{e^{-i\phi}\sin\psi}{\sqrt{3}} \end{pmatrix} \\
& + \theta \begin{pmatrix} -\sqrt{\frac{2}{3}}\cos\psi + \frac{e^{i\phi+\frac{2i\pi}{3}}\sin\psi}{\sqrt{6}} + \frac{e^{i\phi}\sin\psi}{\sqrt{6}} & -\frac{1}{\sqrt{6}} - \frac{e^{-\frac{2i\pi}{3}}}{\sqrt{6}} & -\frac{e^{\frac{2i\pi}{3}}\cos\psi}{\sqrt{6}} - \frac{\cos\psi}{\sqrt{6}} - \sqrt{\frac{2}{3}}e^{-i\phi}\sin\psi \\ \frac{e^{i\phi}\sin\psi}{\sqrt{6}} - \frac{e^{i\phi-\frac{2i\pi}{3}}\sin\psi}{\sqrt{6}} & -\frac{1}{\sqrt{6}} + \frac{e^{\frac{2i\pi}{3}}}{\sqrt{6}} & \frac{e^{-\frac{2i\pi}{3}}\cos\psi}{\sqrt{6}} - \frac{\cos\psi}{\sqrt{6}} \\ \sqrt{\frac{2}{3}}\cos\psi - \frac{e^{i\phi-\frac{2i\pi}{3}}\sin\psi}{\sqrt{6}} - \frac{e^{i\phi+\frac{2i\pi}{3}}\sin\psi}{\sqrt{6}} & \frac{e^{-\frac{2i\pi}{3}}}{\sqrt{6}} + \frac{e^{\frac{2i\pi}{3}}}{\sqrt{6}} & \frac{e^{\frac{2i\pi}{3}}\cos\psi}{\sqrt{6}} + \frac{e^{-\frac{2i\pi}{3}}\cos\psi}{\sqrt{6}} + \sqrt{\frac{2}{3}}e^{-i\phi}\sin\psi \end{pmatrix} \\
& + \theta^2 \begin{pmatrix} \frac{1}{4}\sqrt{3}\cos\psi - \frac{1}{4}\sqrt{3}e^{i\phi+\frac{2i\pi}{3}}\sin\psi & \frac{1}{4}\sqrt{3}e^{-\frac{2i\pi}{3}} & \frac{1}{4}\sqrt{3}e^{\frac{2i\pi}{3}}\cos\psi + \frac{1}{4}\sqrt{3}e^{-i\phi}\sin\psi \\ \frac{1}{4}\sqrt{3}e^{i\phi-\frac{2i\pi}{3}}\sin\psi - \frac{1}{4}\sqrt{3}\cos\psi & -\frac{1}{4}\sqrt{3}e^{\frac{2i\pi}{3}} & -\frac{1}{4}\sqrt{3}e^{-\frac{2i\pi}{3}}\cos\psi - \frac{1}{4}\sqrt{3}e^{-i\phi}\sin\psi \\ 0 & 0 & 0 \end{pmatrix},
\end{aligned} \tag{D1}$$

whereas the deviations in the mixing angles caused by the perturbation θ are accounted for by

$$\sin^2 \theta_{12} = \frac{\left(-\frac{3\theta^2}{8} + \frac{\theta}{2\sqrt{2}} + \frac{1}{2}\right)^2 + \left(-\frac{1}{8}\sqrt{3}\theta^2 - \frac{\theta}{2\sqrt{6}} - \frac{1}{2\sqrt{3}}\right)^2}{f(\theta, \psi, \phi)}, \quad (\text{D2})$$

$$\begin{aligned} \sin^2 \theta_{13} = & \left(\left(-\frac{1}{8}\sqrt{3}\theta^2 - \frac{\theta}{2\sqrt{6}} - \frac{1}{2\sqrt{3}}\right) \cos(\psi) + \left(\frac{\sqrt{3}\theta^2}{4} - \sqrt{\frac{2}{3}}\theta + \frac{1}{\sqrt{3}}\right) \sin(\psi) \cos(\phi) \right)^2 \\ & + \left(\left(\frac{3\theta^2}{8} - \frac{\theta}{2\sqrt{2}} - \frac{1}{2}\right) \cos(\psi) - \left(\frac{\sqrt{3}\theta^2}{4} - \sqrt{\frac{2}{3}}\theta + \frac{1}{\sqrt{3}}\right) \sin(\psi) \sin(\phi) \right)^2, \end{aligned} \quad (\text{D3})$$

$$\begin{aligned} \sin^2 \theta_{23} = & \frac{\left(\left(\frac{\sqrt{3}\theta^2}{8} - \frac{1}{2}\sqrt{\frac{3}{2}}\theta - \frac{1}{2\sqrt{3}}\right) \cos(\psi) + \left(\frac{1}{\sqrt{3}} - \frac{\sqrt{3}\theta^2}{4}\right) \sin(\psi) \cos(\phi) \right)^2}{f(\theta, \psi, \phi)} \\ & + \frac{\left(\left(\frac{3\theta^2}{8} - \frac{\theta}{2\sqrt{2}} + \frac{1}{2}\right) \cos(\psi) - \left(\frac{1}{\sqrt{3}} - \frac{\sqrt{3}\theta^2}{4}\right) \sin(\psi) \sin(\phi) \right)^2}{f(\theta, \psi, \phi)}, \end{aligned} \quad (\text{D4})$$

$$\begin{aligned} f(\theta, \psi, \phi) = & - \left\{ \left(-\frac{1}{8}\sqrt{3}\theta^2 - \frac{\theta}{2\sqrt{6}} - \frac{1}{2\sqrt{3}}\right) \cos \psi + \left(\frac{\sqrt{3}\theta^2}{4} - \sqrt{\frac{2}{3}}\theta + \frac{1}{\sqrt{3}}\right) \sin \psi \cos \phi \right\}^2 \\ & - \left\{ \left(\frac{3\theta^2}{8} - \frac{\theta}{2\sqrt{2}} - \frac{1}{2}\right) \cos(\psi) - \left(\frac{\sqrt{3}\theta^2}{4} - \sqrt{\frac{2}{3}}\theta + \frac{1}{\sqrt{3}}\right) \sin \psi \sin \phi \right\}^2 + 1. \end{aligned} \quad (\text{D5})$$

Appendix E: Computation of radiative decays $l \rightarrow l' \gamma$

The branching ratio of $l \rightarrow l' \gamma$ is

$$\text{Br}(l \rightarrow l' \gamma) = \frac{\tau_l \alpha_{\text{EM}} m_l^5}{64\pi^4} (|c_L|^2 + |c_R|^2), \quad (\text{E1})$$

where the Wilson coefficients $c_{L,R}$ are calculated up to order two. Because of the strong hierarchy in the Yukawa couplings in our model $|y_{ll'}| \gg |y_{ll}|$ the contributions from c_L to $\text{Br}(l \rightarrow l' \gamma)$ can be neglected. The one-loop expressions corresponding to the diagrams in Fig. 1 are given by [38]

$$c_R^{\text{1Loop}} \simeq \frac{1}{4m_l} \int_0^1 \delta(1-u-v-w) \frac{v w m_l y_{l'l} y_{ll}^* + (u+v) m_l y_{l'l} y_{ll}}{w m_s^2 - v w m_l^2 + (u+v) m_l^2 - u v q^2} du dv dw \quad (\text{E2})$$

with $s = h, H, \eta_I, \phi_{a,R}, \phi_{a,I}$. Specifically in the case of $\mu \rightarrow e \gamma$ the two-loop contributions with a top quark and a W boson running in the loop have to be taken into account as they can dominate the cross section in certain regions of the parameter space [38, 39]. The top-loop analytical expressions are

$$c_R^{t\gamma} = -\frac{8}{3} \kappa \frac{v}{m_t} y_{\mu\tau} [\text{Re}(y_{tt}) f(z_{ts}) - i \text{Im}(y_{tt}) g(z_{ts})], \quad (\text{E3})$$

$$c_R^{tZ} = -4\kappa \frac{(1-4s_{\theta_W}^2)(1-\frac{8}{3}s_{\theta_W}^2)v}{16s_{\theta_W}^2 c_{\theta_W}^2} y_{\mu\tau} [\text{Re}(y_{tt}) \tilde{f}(z_{ts}) - i \text{Im}(y_{tt}) \tilde{g}(z_{ts})] \quad (\text{E4})$$

with $\theta_W \simeq 28.74^\circ$ and

$$f(z) = \frac{z}{2} \int_0^1 \frac{1 - 2x(1-x)}{x(1-x) - z} \log \frac{x(1-x)}{z} dx, \quad (\text{E5})$$

$$g(z) = \frac{z}{2} \int_0^1 \frac{1}{x(1-x) - z} \log \frac{x(1-x)}{z} dx, \quad (\text{E6})$$

$$h(z) = \frac{z}{2} \int_0^1 \frac{1}{z - x(1-x)} \left[1 + \frac{z}{z - x(1-x)} \log \frac{x(1-x)}{z} \right] dx, \quad (\text{E7})$$

$$\tilde{f}(x, y) = \frac{yf(x)}{y-x} + \frac{xf(y)}{x-y}, \quad \tilde{g}(x, y) = \frac{yg(x)}{y-x} + \frac{xg(y)}{x-y}, \quad (\text{E8})$$

$$z_{ij} = \frac{m_i^2}{m_j^2} \quad \text{and} \quad \kappa = \frac{\alpha}{2\sqrt{2}\pi} G_F \frac{v}{m_l}. \quad (\text{E9})$$

The W -loop expressions on the other hand are

$$c_R^{W\gamma} = \kappa y_{\mu\tau} \left[3f(z_{Ws}) + \left(5 + \frac{3}{4}\right)g(z_{Ws}) + \frac{3}{4}h(z_{Ws}) + \frac{f(z_{Ws}) - g(z_{Ws})}{2z_{Ws}} \right], \quad (\text{E10})$$

$$\begin{aligned} c_R^{WZ} = \kappa \frac{1 - 4s_{\theta_W}^2}{4s_{\theta_W}^2} y_{\mu\tau} & \left[\frac{1}{2}(5 - t_{\theta_W}^2) \tilde{f}(z_{ts}, z_{WZ}) + \frac{1}{2}(7 - 3t_{\theta_W}^2) \tilde{g}(z_{ts}, z_{WZ}) \right. \\ & \left. + \frac{3}{4}g(z_{ts}) + \frac{3}{4}h(z_{ts}) + \frac{1}{4z_{ts}}(1 - t_{\theta_W}^2)(\tilde{f}(z_{ts}, z_{WZ}) - \tilde{g}(z_{ts}, z_{WZ})) \right]. \end{aligned} \quad (\text{E11})$$

The corresponding diagrams of these loop contributions can be found in, e.g., Fig. 12 of [38].

Appendix F: Loop factors for $h \rightarrow \gamma\gamma$

The dimensionless loop factors $F_{1/2}(\beta)$ and $F_1(\beta)$ (for spin-1/2 and spin-1 particles in the loop, respectively) appearing in Eq. (85) are given by [43, 45]

$$F_{1/2}(\beta) = 2[\beta + (\beta - 1)f(\beta)]\beta^{-2}, \quad (\text{F1})$$

$$F_1(\beta) = -[2\beta^2 + 3\beta + 3(2\beta - 1)f(\beta)]\beta^{-2}, \quad (\text{F2})$$

$$F_0(\beta) = -[\beta - f(\beta)]\beta^{-2}, \quad (\text{F3})$$

with

$$f(\beta) = \begin{cases} \arcsin^2 \sqrt{\beta}, & \text{for } \beta \leq 1 \\ -\frac{1}{4} \left[\ln \left(\frac{1 + \sqrt{1 - \beta^{-1}}}{1 - \sqrt{1 - \beta^{-1}}} \right) - i\pi \right]^2, & \text{for } \beta > 1. \end{cases} \quad (\text{F4})$$

-
- [1] G. Bhattacharyya, P. Leser, and H. Päs, *Phys.Rev.* **D83**, 011701 (2011), 1006.5597.
 - [2] Q.-H. Cao, A. Damanik, E. Ma, and D. Wegman, *Phys.Rev.* **D83**, 093012 (2011), 1103.0008.
 - [3] G. Bhattacharyya, P. Leser, and H. Päs, *Phys.Rev.* **D86**, 036009 (2012), 1206.4202.
 - [4] G. Bhattacharyya, I. de Medeiros Varzielas, and P. Leser, *Phys.Rev.Lett.* **109**, 241603 (2012), 1210.0545.
 - [5] CMS, V. Khachatryan *et al.*, (2015), 1502.07400.
 - [6] A. Dery, A. Efrati, Y. Nir, Y. Soreq, and V. Susić, *Phys.Rev.* **D90**, 115022 (2014), 1408.1371.
 - [7] C.-J. Lee and J. Tandean, (2014), 1410.6803.
 - [8] A. Celis, V. Cirigliano, and E. Passemar, (2014), 1409.4439.
 - [9] D. Aristizabal Sierra and A. Vicente, *Phys.Rev.* **D90**, 115004 (2014), 1409.7690.
 - [10] J. Heeck, M. Holthausen, W. Rodejohann, and Y. Shimizu, (2014), 1412.3671.
 - [11] I. Dorsner *et al.*, (2015), 1502.07784.
 - [12] A. Crivellin, G. D'Ambrosio, and J. Heeck, (2015), 1503.03477.
 - [13] L. Hall and G. Ross, *JHEP* **1311**, 091 (2013), 1303.6962.
 - [14] F. Bazzocchi and L. Merlo, *Fortsch.Phys.* **61**, 571 (2013), 1205.5135.
 - [15] C. Lam, *Phys.Rev.* **D78**, 073015 (2008), 0809.1185.
 - [16] F. Bazzocchi and S. Morisi, *Phys.Rev.* **D80**, 096005 (2009), 0811.0345.
 - [17] H. Ishimori and T. Kobayashi, *JHEP* **1110**, 082 (2011), 1106.3604.
 - [18] S. Morisi and E. Peinado, *Phys.Rev.* **D81**, 085015 (2010), 1001.2265.
 - [19] R. Krishnan, P. Harrison, and W. Scott, *JHEP* **1304**, 087 (2013), 1211.2000.
 - [20] R. Krishnan, *J.Phys.Conf.Ser.* **447**, 012043 (2013), 1211.3364.
 - [21] R. Mohapatra and C. Nishi, *Phys.Rev.* **D86**, 073007 (2012), 1208.2875.
 - [22] R. González Felipe, H. Seródio, and J. P. Silva, *Phys.Rev.* **D87**, 055010 (2013), 1302.0861.
 - [23] V. Keus, S. F. King, and S. Moretti, *JHEP* **1401**, 052 (2014), 1310.8253.
 - [24] F. Wang and Y.-X. Li, *Eur.Phys.J.* **C71**, 1803 (2011), 1103.6017.
 - [25] A. Machado, J. Montero, and V. Pleitez, *Phys.Lett.* **B697**, 318 (2011), 1011.5855.
 - [26] ATLAS, (2012).
 - [27] CMS, C. Collaboration, (2012).
 - [28] A. E. Cárcamo Hernández, I. de Medeiros Varzielas, S. Kovalenko, H. Päs, and I. Schmidt, *Phys.Rev.* **D88**, 076014 (2013), 1307.6499.
 - [29] M. D. Campos, A. E. Cárcamo Hernández, S. Kovalenko, I. Schmidt, and E. Schumacher, *Phys.Rev.* **D90**, 016006 (2014), 1403.2525.
 - [30] A. E. Cárcamo Hernández and R. Martinez, (2015), 1501.05937.
 - [31] A. E. Cárcamo Hernández and R. Martinez, (2015), 1501.07261.
 - [32] Particle Data Group, K. Olive *et al.*, *Chin.Phys.* **C38**, 090001 (2014).
 - [33] D. Forero, M. Tortola, and J. Valle, *Phys.Rev.* **D90**, 093006 (2014), 1405.7540.
 - [34] A. E. Cárcamo Hernández and I. d. M. Varzielas, (2014), 1410.2481.
 - [35] K. Bora, *J.Phys.* **2**, 2013 (2012), 1206.5909.
 - [36] Particle Data Group, J. Beringer *et al.*, *Phys.Rev.* **D86**, 010001 (2012).
 - [37] MEG, J. Adam *et al.*, *Phys.Rev.Lett.* **110**, 201801 (2013), 1303.0754.
 - [38] R. Harnik, J. Kopp, and J. Zupan, *JHEP* **1303**, 026 (2013), 1209.1397.
 - [39] D. Chang, W. Hou, and W.-Y. Keung, *Phys.Rev.* **D48**, 217 (1993), hep-ph/9302267.
 - [40] M. A. Shifman, A. Vainshtein, M. Voloshin, and V. I. Zakharov, *Sov.J.Nucl.Phys.* **30**, 711 (1979).
 - [41] M. Gavela, G. Girardi, C. Malleville, and P. Sorba, *Nucl.Phys.* **B193**, 257 (1981).
 - [42] P. Kalyniak, R. Bates, and J. N. Ng, *Phys.Rev.* **D33**, 755 (1986).
 - [43] J. F. Gunion, H. E. Haber, G. L. Kane, and S. Dawson, *Front.Phys.* **80**, 1 (2000).
 - [44] M. Spira, *Fortsch.Phys.* **46**, 203 (1998), hep-ph/9705337.
 - [45] A. Djouadi, *Phys.Rept.* **459**, 1 (2008), hep-ph/0503173.
 - [46] L. Wang and X.-F. Han, *Phys.Rev.* **D86**, 095007 (2012), 1206.1673.
 - [47] A. E. Cárcamo Hernández, C. O. Dib, and A. R. Zerwekh, *Eur.Phys.J.* **C74**, 2822 (2014), 1304.0286.
 - [48] A. E. Cárcamo Hernández, C. O. Dib, and A. R. Zerwekh, (2015), 1503.08472.
 - [49] CMS, V. Khachatryan *et al.*, *Eur.Phys.J.* **C74**, 3076 (2014), 1407.0558.
 - [50] ATLAS, G. Aad *et al.*, *Phys.Rev.* **D90**, 112015 (2014), 1408.7084.
 - [51] R. Enberg, W. Klemm, S. Moretti, S. Munir, and G. Wouda, (2015), 1502.02931.
 - [52] H. Ishimori *et al.*, *Prog.Theor.Phys.Suppl.* **183**, 1 (2010), 1003.3552.
 - [53] M. E. Peskin and T. Takeuchi, *Phys.Rev.* **D46**, 381 (1992).
 - [54] G. Altarelli and R. Barbieri, *Phys.Lett.* **B253**, 161 (1991).
 - [55] R. Barbieri, A. Pomarol, R. Rattazzi, and A. Strumia, *Nucl.Phys.* **B703**, 127 (2004), hep-ph/0405040.
 - [56] R. Barbieri, (2007), 0706.0684.
 - [57] A. E. Cárcamo Hernández, S. Kovalenko, and I. Schmidt, (2015), 1503.03026.
 - [58] M. Baak and R. Kogler, p. 349 (2013), 1306.0571.
 - [59] M. Baak *et al.*, *Eur.Phys.J.* **C72**, 2205 (2012), 1209.2716.

- [60] M. Baak *et al.*, Eur.Phys.J. **C72**, 2003 (2012), 1107.0975.